Journal of Materials Chemistry A

Accepted Manuscript

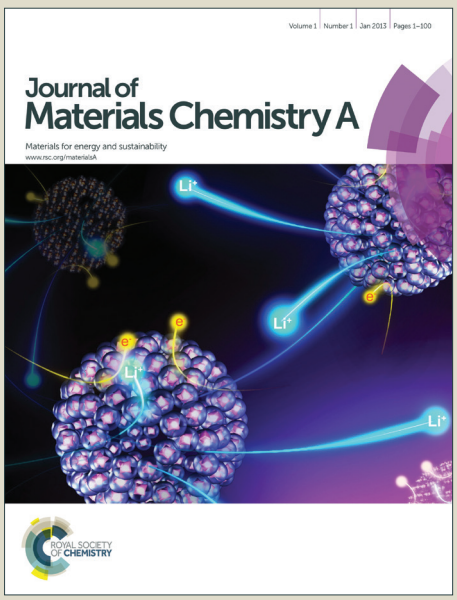

ROYAL SOCIETY OF CHEMISTRY

www.rsc.org/materialsA

Synthesis of Micro and Nano-Sized Calcium Carbonate Particles and Their Applications

Yash BOYJOO, Vishnu K. PAREEK and Jian LIU*
Department of Chemical Engineering
Curtin University
Perth, WA, 6845, Australia

* Author to whom correspondence should be addressed. (J. Liu) E-mail: jian.liu@curtin.edu.au

Abstract

Calcium carbonate nano and micro particles have a large number of industrial applications due to their beneficial properties such as high porosity, high surface area to volume ratio, non-toxicity and biocompatibility towards bodily fluids. Consequently, there has been a significant research to deliver easy ways of synthesising nano and micro sized calcium carbonate particles at specific sizes, polymorphs and morphologies. A majority of its synthesis approaches are based on either the biomimetic or the CO_2 bubbling methods. This review paper describes these methods, and the effects of experimental parameters such as additive types and concentration, pH, temperature, $[Ca^{2+}]$:$[CO_3^{2-}]$ ratio, solvent ratio, mixing mode and agitation time on the properties of the particles produced. The current and potential uses of calcium carbonate particles in areas such as material filling, biomedical, environmental and the food industry have also been discussed.

1. Introduction

The design of functional nano and micro sized materials receives a significant attention due to their applications in the industrial and biotechnological field. The nano- or micro- sized particles not only offer significantly enhanced surface area and volume for better mass and energy transfer but also provide opportunity for material confinement, which can then facilitate chemical reactions in a controlled manner. The materials can be tailored so as to accommodate or react with specific substances and for targeted delivery via electrostatic, pH or temperature dependent interactions. Moreover, the material can be dispersed in small quantities into other materials' matrices so as to improve their chemical or physical characteristics.

Calcium carbonate ($CaCO_3$) is an extremely important material, both in the fundamental research and industry. It has been used as a filler material for paints, pigments, coatings, paper and plastics and can be moulded by organisms into complex and beautiful shapes as in bones, teeth and shells. $CaCO_3$ can exist in mainly four polymorphs: calcite, vaterite, aragonite and amorphous calcium carbonate (ACC), out of which calcite is the most thermodynamically stable phase. The ACC phase is unstable and relatively short-lived and acts as a seed for crystal growth of the other polymorphs. Calcite, vaterite and aragonite have typical morphologies (shapes) which are rhombohedral, spherical and needle-like respectively. Figure 1 shows the typical morphologies of the different $CaCO_3$ polymorphs.

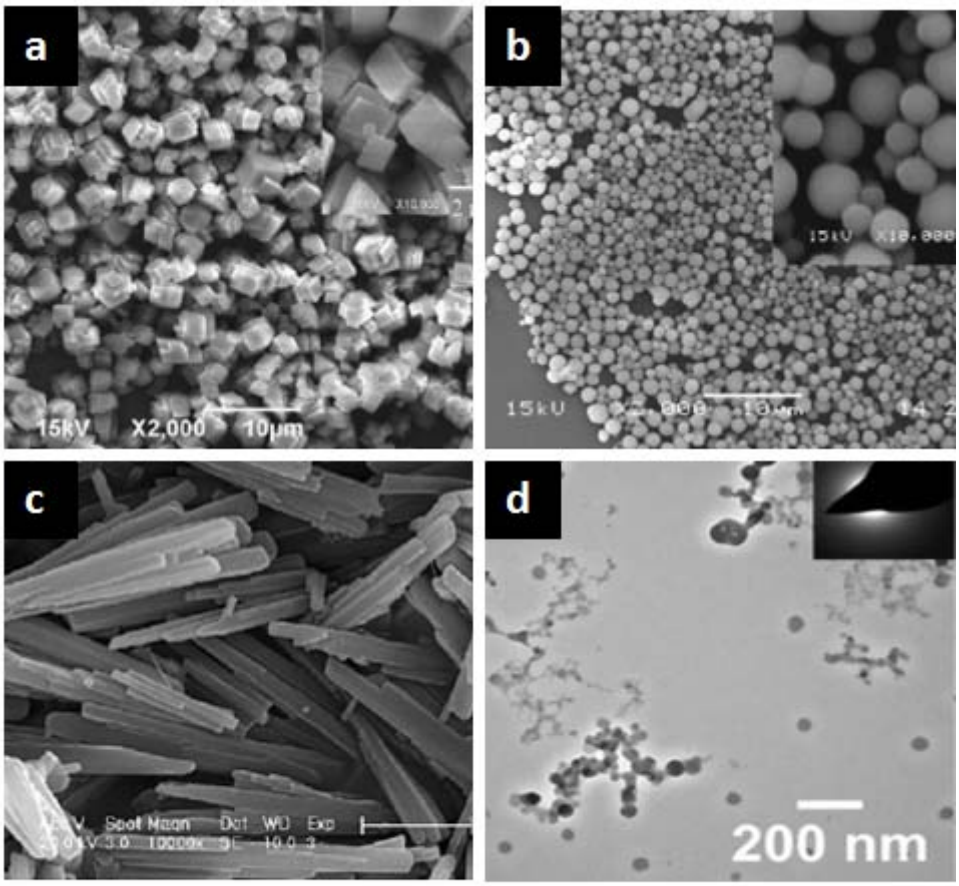

Figure 1: Typical morphologies of the different $CaCO_3$ polymorphs: a) rhombohedral calcite, b) spherical vaterite, c) rod-like aragonite and d) ACC seeds. a) and b) reprinted with permission from ref. [1], c) reprinted with permission from ref. [2] and d) reprinted with permission from ref. [3].

The worldwide availability of $CaCO_3$ (as limestone), compatibility and non-toxicity towards the human body makes the synthesis of this material an interesting and attractive topic for scientists and researchers to delve into. Therefore, countless research have been undertaken so as to stabilise specific $CaCO_3$ polymorphs at different sizes and with exotic morphologies, as shown in Figure 2. Two main synthesis methods exist for such purpose: biomimetic method and CO_2 bubbling method. The former method attempts to imitate nature's ability to synthesise various shapes and sizes by the use of soluble organics and physiological parameters. CO_2 bubbling into slaked lime is the current industrial synthesis method. The $CaCO_3$ particles synthesised as such have various beneficial properties and therefore can have numerous additional uses compared to its current use as a filler material, for example, catalysis, drug delivery vehicles, templates for other functional materials and biosensors. Such characteristics are very much sought after for employment in the

biomedical, environmental and industrial field. Figure 3 depicts the different properties of $CaCO_3$ particles along with the corresponding applications.

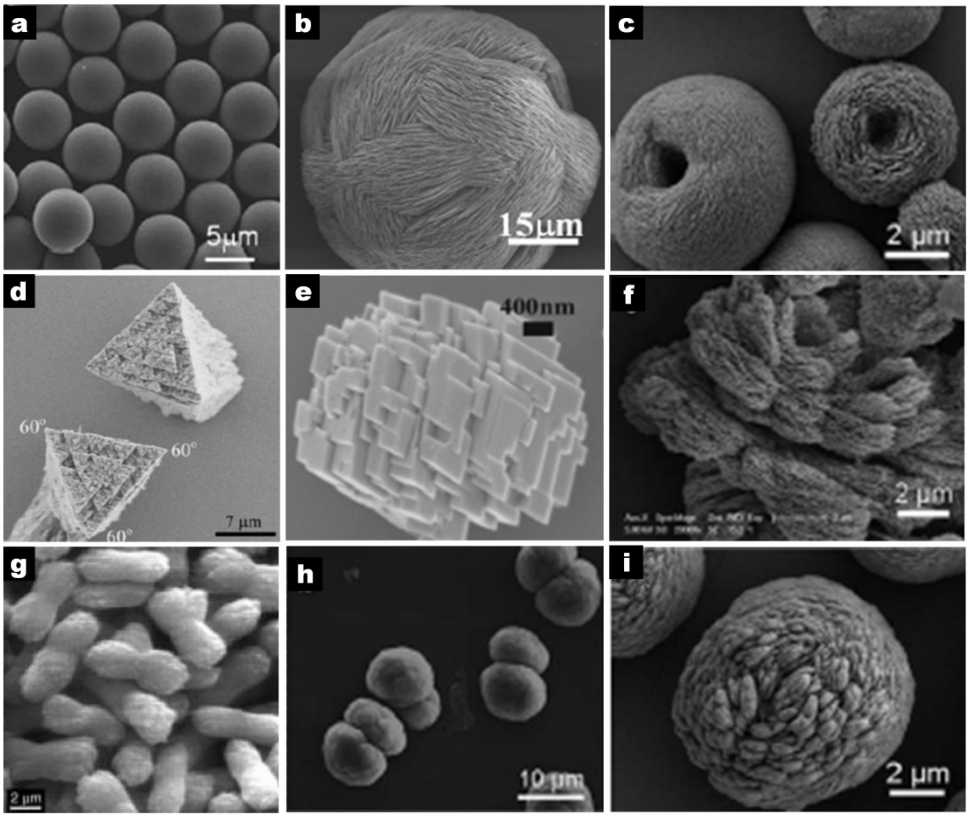

Figure 2: Different shapes that can be exhibited by $CaCO_3$: a) monodispersed spheres, b) sphere with intercrossing pancakes, c) spheres with central cavity, d) pyramid like superstructure, e) laminated cubed shape, f) layered porous hierarchical structures, g) peanut like, h)) twin breaded structures and i) layered irregular spheres. a) reprinted with permission from ref. [4], b) reprinted with permission from ref. [5], c), f), h) and i) reprinted with permission from ref. [6], d) reprinted with permission from ref. [7], e) reprinted with permission from ref. [8] and g) reprinted with permission from ref. [9].

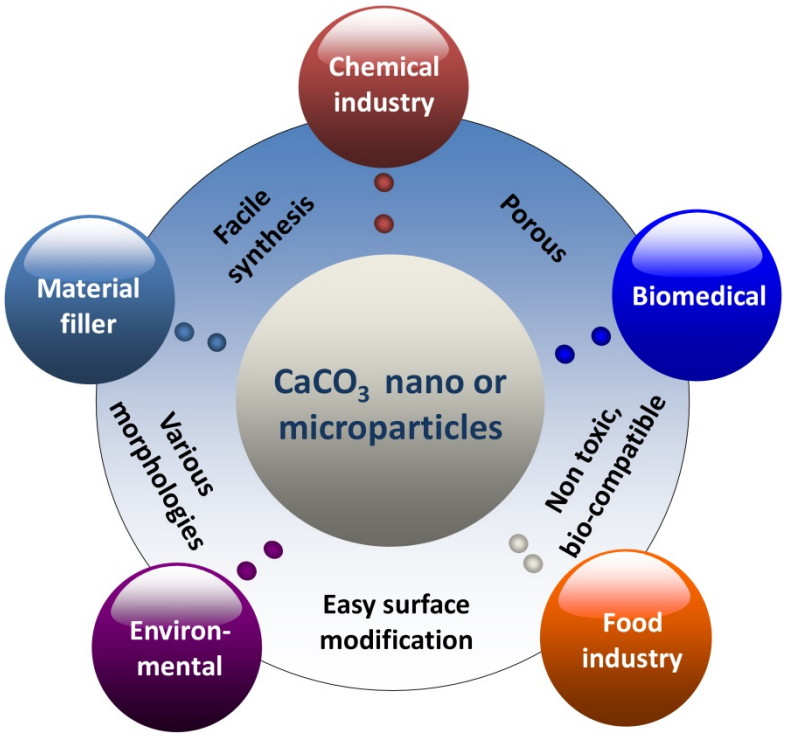

Figure 3: Properties and applications of $CaCO_3$ particles

This review will highlight the main synthesis methods for $CaCO_3$ micro and nano particles. We will examine the effects of various types of additives such as surfactants, polymers and macromolecules, as well as physical and chemical parameters (*e.g.* temperature, solvent ratio and pH) on the $CaCO_3$ sizes, polymorphs and morphologies that have been achieved. We will then look at the current and potential uses of such materials in the materials, chemical industry, biomedical, food industries and environmental.

2. Calcium carbonate synthesis methods

This section will describe the main synthesis methods of $CaCO_3$ particles: biomimetic synthesis and CO_2 bubbling method. Biomimetic method attempts to imitate nature's ability to control the size, shape and phase of $CaCO_3$ using organic compounds which act as templates or growth modifiers as well as other physiological parameters. The latter being the main method for industrial scale production. The description of biomimetic synthesis will be divided into two approaches: (1) the precipitation method; and (2) the reverse emulsion method. Moreover the precipitation method will be further subdivided into the spontaneous precipitation reaction and the slow carbonation reaction. The effects of different experimental parameters on the size, polymorphs and morphology of the obtained particles will be

described. The main $CaCO_3$ synthesis methods are shown in Figure 4. Some other synthesis methods, that are less commonly used, will be also briefly mentioned in this section.

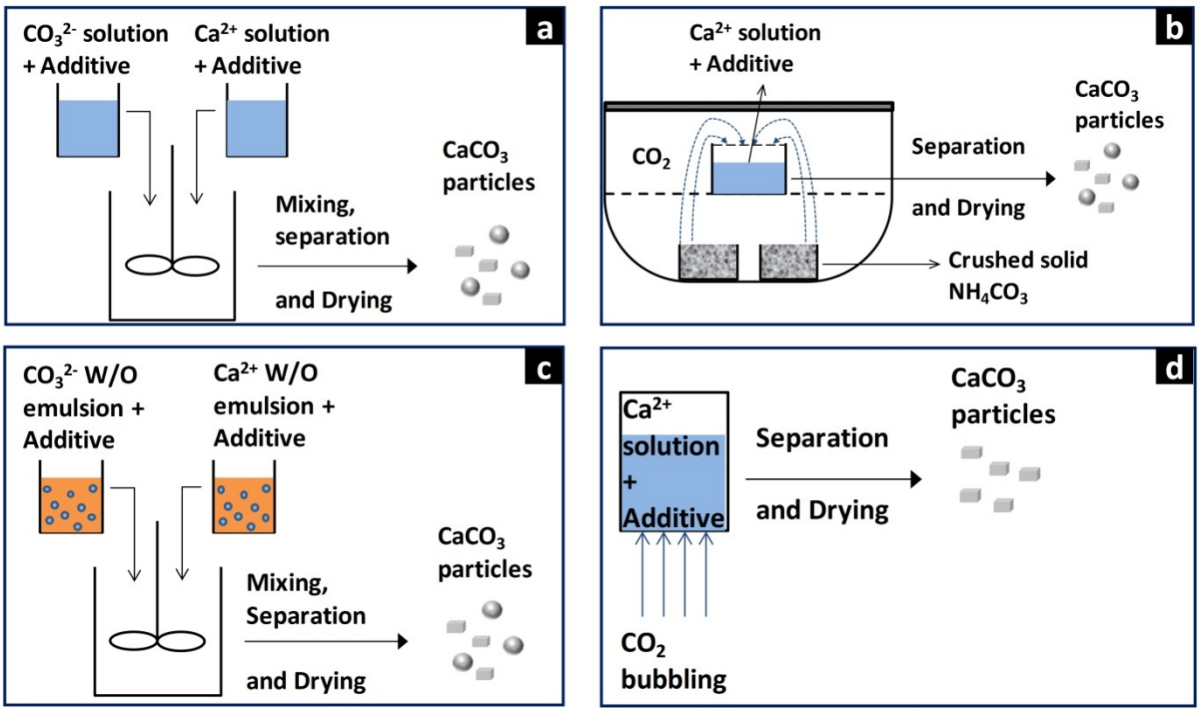

Figure 4: Main $CaCO_3$ synthesis method: a) spontaneous precipitation method, b) slow carbonation method, c) reverse (W/O) emulsion method and d) CO_2 bubbling method. Biomimetic method is represented by a), b) and c).

2.1 Biomimetic synthesis of calcium carbonate

Biomimetic synthesis is an attempt to mimic the elegant ability of nature to synthesise complex and remarkable solid forms out of dissolved materials under mild conditions such as near neutral pH and low temperatures. Some examples are shells in marine animals, as illustrated in Figure 5, who use the transient ACC phase to build their mature crystalline mineral phase [10-12]. Nature uses biomolecules and ions to produce nuclei and then direct and build the nuclei into various shapes. As a result, researchers have used this idea to manufacture various types of particle morphologies, polymorphs and sizes *via* the use of additives. Biomimetic synthesis is easy to implement, requires low quantity of additive (ppm or g L^{-1}) which does not alter the chemical properties of the $CaCO_3$ and displays a vast array of results due to the sheer number of organic additives that exist. $CaCO_3$, which has three crystalline phases (vaterite, aragonite, and calcite) and an unstable amorphous phase, is one of the most studied systems for its important role in understanding the natural mechanism of biomineralisation and designing new composite materials. It is well-accepted that the ACC is a transient precursor phase of biogenic crystalline ones in biomineralisation; some acid-rich

glycoproteins can stabilise ACC efficiently and regulate its transformation into crystalline forms.

Figure 5: Examples of $CaCO_3$ occurring in nature: mollusc shells [13].

The functions of the additives are to interact with the Ca^{2+} ions and provide active sites for nucleation of $CaCO_3$ which then agglomerate into nano or micro particles. At the same time, the additives bond to preferential surfaces of the crystals to prevent further growth in specific planes. This enables the stabilisation of the metastable phases, vaterite, aragonite, and ACC crystallites as well as the stabilisation of different kinds of morphologies such as spheres, hollow spheres, dumbbells, peanut-like, flower-like, pine-cones, pancakes, spindles *etc*.

Various types of additives such as surfactants, polyelectrolytes, double hydrophilic block copolymers (DHBC), triblock copolymer, polysaccharides such as soluble starch and protein based additives such as amino acids, bovine serum albumin (BSA), dopamine and amino carboxyl chelating agent have been used as biomimetic agent to achieve different particle morphologies, polymorphs and sizes.

The main synthesis methods as well as the effect that the controllable experimental parameters have on the characteristics of the final product will be discussed in this section.

2.1.1 Precipitation method

Biomimetic precipitation reaction methods include the spontaneous precipitation reaction and the slow carbonation reaction. Spontaneous precipitation reaction is the main and easiest way

to prepare $CaCO_3$ particles as it basically involves the mixing of CO_3^{2-} and Ca^{2+} solutions containing the additives. There are, however some nuances regarding the experimental procedure and controllable parameters as will be explained next. In slow carbonation reaction CO_3^{2-} ions are produced from the dissolution of CO_2 gas that is formed *via* the slow hydrolysis of an additive such as dimethyl carbonate (DMC) or ammonium carbonate ($(NH_4)_2CO_3$) in alkaline condition. The typically long reaction times involved in slow carbonation reaction can sometimes achieve some striking hierarchical structures.

2.1.1.1 Effect of additive type and concentration

The effects of the different types of additives on the morphology, polymorph and size of $CaCO_3$ particles are summarised in Table 1 and Table 2 for spontaneous precipitation and carbonation precipitation respectively, which are discussed thereafter.

Table 1: Effects of additives on morphology, polymorph and size of $CaCO_3$ particles via spontaneous precipitation at $[Ca^{2+}]:[CO_3^{2-}]$ ratio = 1:1 and near room temperature

C – Calcite, L – Length, V – Vaterite, W – Width, NA – Not Applicable, NR – Not reported, * - Assumed room temperature used in the experiments

			Experimental Conditions				Results		
Ref.	**Additive(s)**	**Additive(s) Type**	**Additive(s) Concentration(s)**	**Reaction Time (h)**	**pH**	**Temp (°C)**	**Morphology**	**Polymorph**	**Size (μm)**
14	None	N/A	N/A	0.0083	NR	25*	Spheres	C	4-6
15	DTAB	Surfactant	12.5-20 mmol L^{-1}	48	11	25	Multi petal flowers	C	0.6-0.8
8	DDAB, $[C_{12}mim]Br$	Surfactants	5 mmol L^{-1} DDAB + 7.5-20 mmol L^{-1} $[C_{12}mim]Br$	48	NR	25	Flower shaped	NR	0.3 (Petal length)
16	SDS	Surfactant	5 mM	10	7	26	Spheres	C	3-4
17, 18	PSS	Polyelectrolyte	4 g L^{-1}	NR	NR	25*	Spheres	NR	4-6
19	PSSS	Polymer	1 g L^{-1}	12	10	25*	Spheres	94%C, 6%V	8
20	PS-*b*-PAA	Polymer	1.28 M	0.5	NR	30	Spheres	C	2
21	PAMPSAA	Polymer	0.05 wt%	0.5	9	25*	Spheres	37.3%C, 62.7%V	8-10
22	PAA	Polymer	1 g L^{-1}	24	9	25	Plate like aggregates	C	4-8
23	PAAL	Block Copolymer	0.4 g L^{-1}	48	10	25*	Spheres	C, V	5
24	PEG-*b*-PMAA	DHBC	0.2 g L^{-1}	24	10	22	Peanut like	C	6.4L, 2.1W
25	PS-*b*-PAA-*b*-PEG	Triblock Copolymer	0.5 g L^{-1}	24	10	25*	Hollow Spheres	C	0.03
26	$(EO)_{20}$-$(PO)_{72}$-$(EO)_{20}$	Amphiphilic Triblock Copolymer	1 g L^{-1}	24	11	25	Spheres	58%C, 42%V	1.6
	HPCHS	Chitosan	1 g L^{-1}				Rhombohedral	C	4.7
27	NR	Soluble starch	1x10^{-3} wt%	24	NR	30	Hollow Spheres	V	0.5
28	4-BAPTA	Amino carboxyl chelating agent	1 mM	72	9	25*	Spheres + Rhombodedrals	>80% V	3
29	DNA	Amino Acid	1 g L^{-1}	24	10.5	25*	Spheres	C	14
30	BSA	Amino Acid	Langmuir monolayer (thin film)	2	NR	25	Kayak like	C	20L, 5W
31	PVP, SDBS	Polymer, Surfactant	100 g L^{-1} PVP	10	NR	26	Rhombohedral	C	5-6
			5x10^{-2} M SDBS				Spheres	V	2-4
			100 g L^{-1} PVP + 5x10^{-2} M SDBS				Schistose	C, V	3-5

[32]	PSMA, CTAB	Polymer, Surfactant	0.5 g L^{-1} PSMA + 1 mM CTAB	24	10	25*	Hollow Spheres	96%C, 4%V	2-3
[33]	PVP, SDS	Polymer, Surfactant	10 g L^{-1} PVP + 10 mM SDS	1	NR	20	Hollow Spheres	C	2-3
[34]	PEG, SDS	Polymer, Surfactant	1 g L^{-1} PEG + 3.5 mM SDS	24	NR	25*	Hollow Spheres	C,V	3-6
[35]	PEO-*b*-PMAA, SDS, CTAB	DHBC, Surfactants	1 g L^{-1} DHBC + 1-2 mM SDS	24	10	22	Hollow Spheres	C	3.4
			2 g L^{-1} DHBC + 1 mM CTAB				Pine Cone	C	3L, 1.2D
[36]	Pluronic F127, SDS	Triblock Copolymer, Surfactant	2 g L^{-1} F127 + 20 mM SDS	1	NR	30	Hollow Spheres	C	3-4

Table 2: Effects of additives on morphology, polymorph and size of $CaCO_3$ particles via carbonation precipitation

ACC – Amorphous calcium carbonate, C – Calcite, V – Vaterite, NR – Not reported, * - Assumed room temperature or pH used in the experiments

			Experimental Conditions						Results		
Ref	**Additive**	**Additive Type**	**Additive Conc**	**Ca conc (mM)**	**CO_2 source**	**Temp (°C)**	**pH**	**Reaction time (h)**	**Morphology**	**Polymorph**	**Size (µm)**
[37]	AE 3007	Surfactant	NR	10	DMC	15	11*	Few hours	Spherical	NR	0.759
						20					0.595
						30					0.475
[5]	p-aminobenzene sulfonic acid + L-Lys	Surfactants	0.1 g L^{-1}:0.5 g L^{-1}	10	$(NH_4)_2CO_3$	25*	4	48	Thick pancake	C	40-75
			0.1 g L^{-1}:0.5 g L^{-1}				8		Thin pancake	C + V	ca. 30-60
			0.1 g L^{-1}:0.5 g L^{-1}				9		Spheres of intercrossing hexagonal shapes	V	18
			0.1 g L^{-1}:10 g L^{-1}				7.5		Spheres of intercrossing pancake shapes	V	60
			0.1 g L^{-1}:10 g L^{-1}	30			8		Lens	V	ca.8
[38]	PAA	Polymer	20 ppm	20	$(NH_4)_2CO_3$	23	9.3	4	Spherical	ACC	1
								10	Hollow spheres	V	1
[7]	PSMA	Amphiphilic polymer	0.1 g L^{-1}	1.25	$(NH_4)_2CO_3$	22	NR		Pyramid	C	
								168			ca. 15
[39]	PSS	Polyelectrolyte	NR	10	DMC	20	12	1.5	Spherical	ACC	0.08
[40]	Egg-white	Protein	0.015 g ml^{-1}	300	$(NH_4)_2CO_3$	28	NR	3-<6	Platelet like	V	ca. 1-2
								6-36	Wool sphere-like	V	ca. 40-90
[41]	Phytic acid	Saturated cyclic acid	1 g L^{-1}	10	$(NH_4)_2CO_3$	25*	3	120	Hollow spheres	ACC	1-2.8
[42]	DMC	Carbonate ester	20 mM DMC	20	DMC	20	11*	0.33	Spherical	ACC	0.79
			60 mM DMC						Spherical	ACC	0.43

No additives

Highly porous, homogeneous spherical microparticles of calcite could be produced without additives (instead of typical rhombohedral crystals) from supersaturated (relative to $CaCO_3$) solution and very rapid mixing [14, 43]. The intense agitation of 0.33 M Na_2CO_3 and 0.33 M $CaCl_2$ solutions for 30 s resulted in microspheres with an average diameter ranging from 4 to 6 μm [14]. The diameter of the particles could increase to 15-20 μm with increasing reaction time [43]. The morphology and porosity of the microspheres produced through rapid mixing without additives are shown in Figure 6.

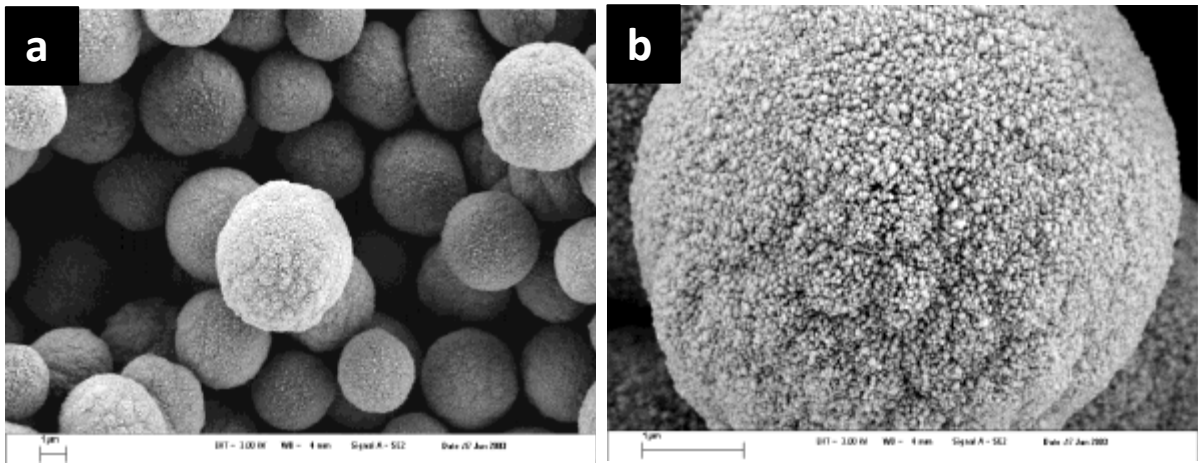

Figure 6: a) SEM of microspheres synthesised without additives, b) SEM of one microsphere showing the porous nature of the particle. Reprinted with permission from ref. [43].

Surfactants

As shown in Table 1, Wei *et al.* [16] compared the influence of three anionic surfactants (sodium dodecylsulfate (SDS), sodium dodecylbenzene sulfonate (SDBS) and sodium dodecylsulfonate (DDS)) having the same hydrophobic alkyl chains but different head groups on the crystallisation habit of $CaCO_3$. They found that DDS did not greatly affect $CaCO_3$ morphology with increasing DDS concentration. However, 5 mM SDS could result in monodispersed hollow spheres of calcite of 3-4 μm in size while 5 mM SDBS synthesise monodispersed vaterite spheres within size range of 1-3 μm. SDS and SDBS, being at concentrations larger than the critical micelle concentration (CMC) values, formed micelles that were covered by $CaCO_3$ nuclei *via* electrostatic interaction and this eventually led to formation of spherical particles. The formation of hollow spheres was attributed to the "bubble effect" of SDS in solutions. The favouring of one phase over another was attributed to the surfactant orientation and strength of electrostatic attraction between surfactant and

$CaCO_3$ nuclei. The effects of cationic surfactants 1-dodecyl-3-methylimidazolium bromide ($[C_{12}mim]Br$) and didodecyldimethylammonium bromide (DDAB), either individually or mixed together, were also investigated [8, 44]. With $[C_{12}mim]Br$, laminated cube shaped structures and string-like structures, all consisting of calcite, appeared at 15-30 and 60 mmol L^{-1} respectively. With DDAB, the crystalline form converted from laminated cube shaped calcite to spherical vaterite as the surfactant concentration increased from 2.5 to 10 mmol L^{-1}. Mixing those surfactants gave rise to micelles with different induced directions and intensities due to the different head groups. This micellar structure resulted in the formation of flower shaped crystals with 300 nm long petals and made of calcite, at concentrations of 5 mmol L^{-1} $[C_{12}mim]Br$ and 7.5-20 mmol L^{-1} DDAB. Calcite flower shapes diameter in the range 600-800 nm was also obtained with 12.5-20 mmol L^{-1} cationic surfactant dodecyltrimethylammonium bromide (DTAB) [15]. In that case, the flower shape was attributed to the assembling of rod-like basic units. Chen and Nan [45] investigated the effect of mixed cationic/anionic surfactants cetyltrimethylammonium bromide (CTAB)/SDS on $CaCO_3$ produced from the reaction of calcium acetate solution with urea at 90 ºC in an autoclave. At a ratio of 0 (pure SDS), flower shaped vaterite, formed by aggregation of hexagon-like basic units was obtained and at ratio of 0.5, pyramid and sphere shaped structures (also consisting of vaterite) were produced. Aragonite started forming as the ratio further increased. A mixture of aragonite and vaterite was obtained at ratio of 1, while pure aragonite was obtained at a ratio of 5. The crystals formed at higher ratios consisted of cluster shapes aggregated by rods. The effect of surfactant mixing at different ratios was also investigated [5]. The authors found that when p-aminobenzene sulfonic acid and L-lysine were mixed at a ratio of 0.1 g L^{-1}:0.5 g L^{-1} and at a pH of 8, thin pancake morphology of calcite and vaterite mixture was formed and had relatively large size ca. 30-60 μm. With a much higher concentration of L-lysine (0.1 g L^{-1}:10 g L^{-1} ratio) but slightly reduced pH of 7.5, spheres with intercrossing pancakes shapes of vaterite and size of ca. 60 μm were formed. Therefore, changing the ratio of mixed surfactants as additive can have profound effects on the shape, phase and size of the particles produced.

Synthetic polymers

Synthetic polymers, at the right concentration, generally induce the formation of monodispersed vaterite spheres as seen from Table 1, although calcite spheres have been obtained in other cases [20, 44]. Other shapes such as peanut-like calcite and nano-sized hollow calcite spheres could also be synthesized with double hydrophilic block copolymer

poly(ethylene glycol)-*block*-poly(methacrylic acid) (PEG-b-PMAA) [24] and triblock copolymer poly(styrene-*block*-acrylic acid-*block*-ethylene glycol) (PS-b-PAA-b-PEG) [25] respectively. The amount of crystals formed is in the micromolar range although higher concentration of 0.25 M has been successfully synthesised [46]. It can be seen from Table 1 that the sizes of the spheres are in the micron range for additive concentration most usually in the range 1-4 g L^{-1}. The spheres are generally porous with rough surface since they are aggregates of nanoscale crystallites formed in the polymer matrix. The final surface morphology and polymorph of the particles depends on the type of polymer employed. [19] Poly(sodium-4-styrenesulfonate) (PSSS) having molecular weight 1,000,000 was demonstrated to yield monodispersed microsized spheres with surface consisting of many nanocrystals while with PSSS having lower molecular weight of 70,000, microspheres with zigzag surfaces were obtained. Elsewhere [47], it was shown that a triblock copolymer with the longer block length was able to stabilise vaterite crystals unlike its shorter length counterpart, which favoured calcite. This shows that due to the different lengths, the spatial structure of the polymer in the solution was an important factor in determining the polymorphic and morphological characteristics of the particles. Unusual morphologies taken by calcite such as pyramid like superstructures were synthesised [7] by slow carbonation reaction for a period of 7 days in the presence of poly(styrene-alt-maleic acid) (PSMA) amphiphilic polymer as additive. The morphology resulted from self-similar growth of triangular capped units aggregated by nanocrystals subunits resulting from selective adsorption of polymer molecules on the crystals surfaces. Regarding smaller sized particles, nanosized $CaCO_3$ spheres were successfully synthesised [1] using poly(styrenesulfonate) (PSS) and reactants Ca^{2+}:CO_3^{2-} molar ratio of 5:1. They found that as the concentration of PSS increased, the particles became smaller and more uniform in size distribution. At PSS concentration of 50 g L^{-1}, vaterite particles in the size range 400-500 nm were produced.

Biomolecules

Biomolecules such as cellulose, polysaccharide and soluble starch favour the formation of porous vaterite at low additive concentrations [27, 48, 49] as well as increase the crystals specific surface area [48]. The concentration of metastable vaterite was optimised by carefully controlling the concentrations of methyl cellulose (MC), hydroxyethyl cellulose (HEC) FD-10000 and HEC FD-30000 respectively [49]. At 0.05% MC, a mixture of spherical vaterite (4-6 μm diameter) and rhombohedral calcite were formed. The fraction of vaterite in the mixture was 42.5%. Increasing the molecular weight of the cellulose increased the fraction of vaterite.

At ca. 0.05% concentration of HEC FD-10000, 67.3% vaterite was obtained while 80.6% vaterite fraction was obtained with 0.1% concentration of HEC FD-30000. Wei *et al.* [27] used a one pot approach to achieve monodispersed hollow vaterite spheres with diameter of 500 nm by using very dilute solutions of CO_3^{2-} and Ca^{2+} (2 mM) with soluble starch as additive at 30 ºC. However as the concentration of CO_3^{2-} and Ca^{2+} increased to 5 mM and 12.5 mM, the morphology and polymorph changed to calcite cubic aggregates and solid vaterite spheres respectively.

Amino acids

Amino acid or amino acid derivatives have been used to synthesise some other exotic particles. Dopamine at 2 g L^{-1} was found to stabilise highly porous vaterite microspheres following spontaneous precipitation reaction [50]. The spherical vaterite particles were formed within two minutes of reaction and could be preserved for over two months in aqueous solution. Unique spherical superstructure made of calcite that had the surface composed of many triangular shaped prisms and perpendicular to the surface of the spheres were synthesised with 1g L^{-1} deoxyribonucleic acid (DNA) [29]. These particles had relatively uniform diameter of 14 μm. Jujube-nucleus-like and kayak like particles of calcite were synthesised via templating with BSA monolayers after 1 h and 2 h reaction, respectively [30].

Polymer/surfactant mixtures

Some researchers have used the complex micellar templates resulting from polymer/surfactant mixtures to produce other types of morphologies, mainly hollow spheres [32-36, 51, 52]. Fine tuning of the polymer/surfactant concentrations was required to achieve the hollow structure. Yan *et al.* [36] synthesised hollow spheres of aggregated nanoflakes with diameter 3-4 μm and shell thickness of 400 nm from 2 g L^{-1} of triblock copolymer Pluronic F127 and 20 mM SDS (Figure 7a). Increasing the concentration of either the polymer (>4 g L^{-1}) or the surfactant (60 mM) led to an increase in the compactness of the spheres, hence producing solid spheres. Some other types of particles synthesised via polymer/surfactant mixtures include: uniform vaterite convex discs (Figure 7b) and hollow discs (Figure 7c) with a mixed poly(ethylene oxide)-*block*-poly(methacrylic acid) (PEO-b-PMAA)/SDS system after 1 day and 7 days of reaction respectively [35], uniform pine cone calcite shapes (Figure 7d) with a mixed PEO-b-PMAA/CTAB system [35] and mixed calcite and vaterite schistose structures with a mixed polyvinylpyrrolidone (PVP)/SDBS system [31].

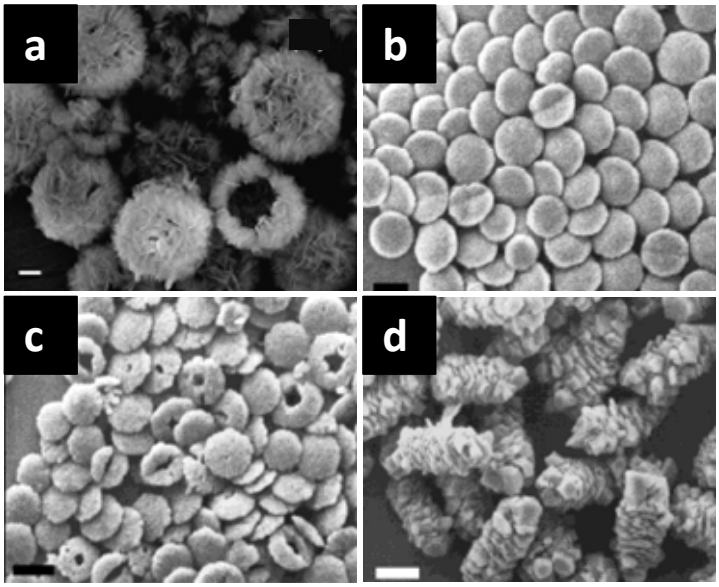

Figure 7: a) hollow spheres with 2 gL-1 of triblock copolymer Pluronic F127 and 20 mM SDS, b) convex discs with mixed PEO-b-PMAA/SDS after 1 day, c) hollow discs with mixed PEO-b-PMAA/SDS after 7 days and d) uniform pine cone shapes with mixed PEO-b-PMAA/CTAB system. a) reprinted with permission from ref. [36], b), c) and d) reprinted with permission from ref. [35].

Other additives

Unstable ACC can be stabilised with Mg as inhibitor even though the ACC was kept stable in solution for only two days [53]. However, phytic acid proved to be a much better stabiliser for ACC [41]. The morphology and polymorph of the hollow ACC microspheres formed were effectively kept unchanged even when the products were kept in mother solution for 3 months or in solid state for 1 year.

2.1.1.2 Effect of pH

As can be seen from Table 3, the solution pH can have drastic effects on the morphology, and size of $CaCO_3$ particles formed, but less so on the polymorphism. Controlled crystal growth depends on the degree of interaction between the carboxylic acid groups in the additives and the Ca^{2+} ions in solution. Hence the more the carboxylic groups get ionised, the more sites are available for binding with the Ca^{2+} ions which therefore inhibits crystal growth in all directions. Solution pH influences both the degree of protonation of the carboxylic acid groups and the $CaCO_3$ supersaturation in the solution. The degree of ionization of the carboxylic groups increases with increasing pH [28] but so does the solution supersaturation, due to the hydrocarbonate/carbonate buffer [24]. As a result, a compromise in the pH needs to be found so as to optimise the protonation of the carboxylic groups while at the same time reducing the nucleation rate of the crystals due to high solution supersaturation. From Table 3, the best pH range for controlled crystal growth is generally around 9-11. At high solution

pH the high solution supersaturation overwhelms the degree of ionization of the carboxylic acid groups, which leads to uncontrolled crystal growth and the occurrence of larger sized, irregular shaped particles. Low nucleation rate can also in some cases suppress changes of metastable phases into stable ones, such as vaterite into stable calcite [26, 28, 54, 55] at low temperature or aragonite into vaterite at high temperature [56].

Table 3: Effect of pH on morphology, polymorph and size of $CaCO_3$ particles

C – Calcite, L – Length, V – Vaterite, W – Width, NA – Not applicable, NR – Not reported, * - Assumed room temperature used in the experiments

Ref	Additive(s)	Temp. (°C)	pH	Morphology	Polymorph	Size (μm)
[26]	P123 [$(EO)_{20}$-$(PO)_{72}$-$(EO)_{20}$]	25	10	Spherical	C, V	ca. 1-3
			11	Spherical	58%C, 42%V	1.6
			12	Rhombohedral	C	ca. 2-5
	HPCHS		10	Rhombohedral	C	ca. 1-5
			11	Rhombohedral	C	4.7
			12	Rhombohedral	C	ca. 1-6
[23]	PAAL	25*	9	Spherical	C, V	5-8
			10	Spherical	C, V	5
			11	Spherical + Rhombohedral	C, V	ca. 2-4
			12	Irregular aggregates	C	ca. 5-8
[19]	PSSS + CTAB	25	9	Spherical	NR	10-15
			10	Spherical	94%C, 6%V	8
			11	Spherical + Irregular aggregates	NR	ca. 2-4
			12	Irregular aggregates	NR	ca. 3-6
[15]	DTAB	25	11	Multi petal flowers	C	0.6-0.8
			13	Multi antenna + Wire like	C	2L, 0.13W (Antenna)
[44]	PAA	80	9	Cubic	C	3
			10	Cubic	C	ca. 5-8
			12	Irregular aggregates	C	ca. 3-9
[28]	4-BAPTA	25	7.5	Cubic	C	4.5
			8	Spherical (60%) + Irregular aggregates (40%)	40%C, 60%V	4.2
			9	Spherical + Rhombodedrals	>80% V	3
			11	Rhombohedral	C	3
[22]	PAA	25	9	Plate like aggregates	C	4-8
			10	Spherical + Irregular aggregates	C	ca. 2-8
			11	Spherical + Irregular aggregates	C	ca. 3-10
			12	Irregular aggregates	C	NA
[24]	PEG-*b*-PMAA	22	9	Rod like	C	15L, 2W
			9.5	Dumbbell like	C	5.6L, 1.6W
			10	Peanut like	C	6.4L, 2.1W
			10.5-11	Ellipsoidal + Irregular aggregates	C	2.5 (Ellipsoidal)

Still, some researchers have found some useful crystal morphologies at high pH, due to the type of additive used. Li *et al.* [15] developed high surface area multi-antenna shaped and wire-like structures at pH=13 using DTAB as additive. This morphology was due to the OH^- ions compressing the electrical double-layer around the surfactant ions and inducing the formation of multi-antenna shaped crystals. Mao and Huang [54] developed spindled spherical and peanut aggregates at pH=11.5 using malic acid while peanut, dumbbell and mushroom like shapes were produced at pH=12.6 using polycarboxylate ether copolymers with varying chain lengths [55].

Some reactions at low pH have been investigated via the carbonation pathway (see Table 2). Thick pancakes of calcite and having relatively large size of ca. 40-75 μm were formed at pH=4 using surfactants p-aminobenzene sulfonic acid and L-Lysine at ratio of 0.1 g L^{-1}:0.5 g L^{-1} [5]. Elsewhere, a pH of 3 using phytic acid as additive and a long reaction time of 120 h gave rise to hollow spheres of ACC with size range 1-2.8 μm [41].

2.1.1.3 Effect of temperature

Reaction temperature affects the morphology, polymorph and size of $CaCO_3$ particles. High temperature is indeed the main factor contributing to the formation of aragonite having typical elongated needle/rod-like shape as shown in Table 4. Higher temperature increases the energy of the reactive environment which favours the formation of high surface energy aragonite crystals from the phase transformation of calcite and vaterite.

Table 4: Effect of temperature on morphology, polymorph and size of $CaCO_3$ particles

A – Aragonite, C – Calcite, L – Length, V – Vaterite, W – Width, NA – Not applicable, * - Molar percent reported, ** - Volume percent reported

Ref	Additive	Temp. (°C)	Morphology	Polymorph	Size (μm)
[57]	None	30	Mushroom like lamellar aggregates	1.6%C, 98.4%V*	20-35
		50	Lamellar	10.8%A, 89.2%V*	10-20
		60	Lamellar aggregates	25.4%A, 74.6%V*	ca. 15-40
		80	Rod like	A	(15-40)L, (1-5)W
[15]	DTAB	25	Multi petal flowers	C	0.6-0.8
		60	Coral	47.8%A, 52.2%C	3D
		80	Dendrite	93.2%A, 6.8%C	-
[27]	Soluble starch	15	Hollow Spheres	V	0.3
		30	Hollow Spheres	V	0.5
		50	Hollow Spheres	V	2
		70	Hollow Spheres	V	2.5
[58]	PAA	25	Rhombohedral + Raspberry	49.5%C, 50.5%V**	10-15
		50	Dendrite + Flower like	10.8%A, 10.2%C, 79%V**	5-10

		80	Needle like	89%A, 8.7%C and 1.5%V**	4
[59]	SDC	30	Wafer	V	1-2
		50	Spherical-flower	V	1-2
		120	Spindle	A	10-15
[60]	PAM	25	Stacked rhombohedra	C	ca. 2-3
		80	Aggregated plates + Rods	C	-
	PAA	25	Spherical	C, V	ca. 2-3
		80	Irregular aggregates	C, V	-

Crystal growth in the presence of additives generally increases at elevated temperatures such that, in cases where aragonite is not formed, aggregation of particles occurs [33, 60]. Nevertheless, some researchers [27] used soluble starch to synthesise monodisperse hollow vaterite spheres with increasing size from 300 nm, 500 nm, 2 µm to 2.5 µm at 15, 30, 50 and 70 °C respectively. This was due to the dissolution of crystals from the core and recrystallisation at the surface, even at high temperatures, which was facilitated by the low reactant concentration used (2 mM of Ca^{2+} and CO_3^{2-}). That study showed that $CaCO_3$ concentration had also strong influence in the shape of crystals at different temperatures. With 5 mM Ca^{2+} and CO_3^{2-}, the morphology changed from cubic aggregates to dendrite-like and finally flower shaped crystals as temperature increased while at concentration of 12.5 mM, solid spheres (increasing in diameter as temperature increased) and spindle-like shapes were obtained with increasing temperature (Figure 8).

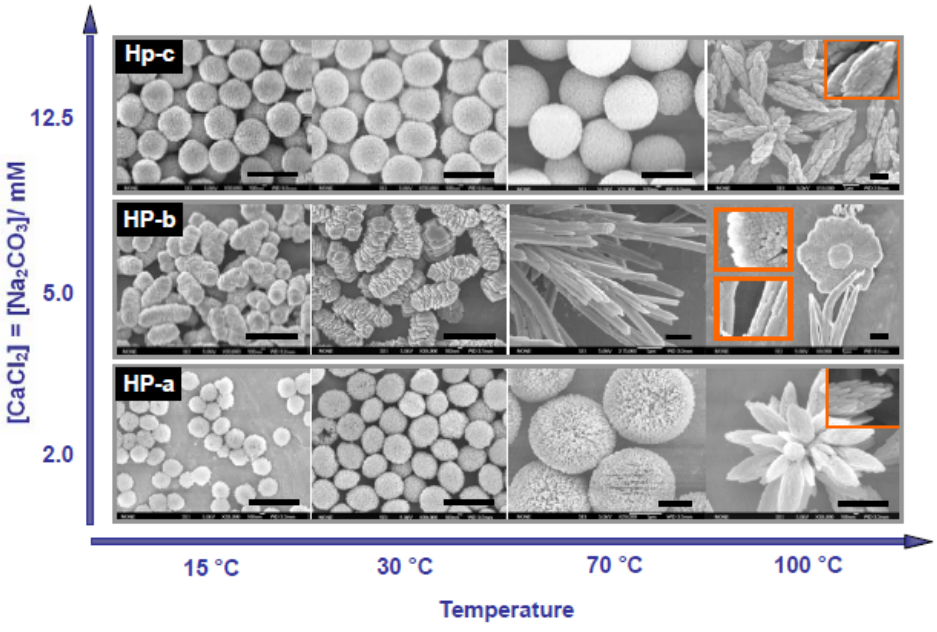

Figure 8: Effect of temperature with starch as additive and at different concentrations of $CaCO_3$. Reprinted with permission from ref. [27].

Temperature changes within room temperature range (< 30 °C) mainly affect the size of the particles. Spontaneous precipitation using soluble starch produced hollow spheres of vaterite with size 0.3 μm and 0.5 μm at 15 °C and 30 °C respectively (see Table 4). The increase in particle size with elevated temperature was observed at all the Ca^{2+} and CO_3^{2-} concentration investigated (2, 5 and 12.5 mM respectively) [27]. However, the opposite trend was observed with carbonation precipitation reaction involving polymer surfactant AE 3007 [37]. In the latter case, the size of the spheres formed decreased with increase in temperature from 15 °C to 30 °C (see Table 2).

When no additives are used, rhombohedral calcite crystals become smaller at elevated temperatures [22, 44] due to the increased solubility of calcite crystals.

2.1.1.4 Effect of $[Ca^{2+}]$:$[CO_3^{2-}]$ ratio

The $[Ca^{2+}]$:$[CO_3^{2-}]$ ratio is an important factor to consider when synthesising $CaCO_3$ particles. Calcium rich solutions are in the pH range 7-8 while carbonate rich solutions are in the range 9.5-10.5 [1]. Higher solution pH results in a higher supersaturated mixture and hence higher nucleation rate of crystals. On the other hand, high calcium content provides a greater number of positively charged sites for electrostatic attraction of negatively charged groups of the organic additives on the crystal surface, which suppresses uncontrolled growth. This explains the higher particle size obtained by some researchers at low $[Ca^{2+}]$:$[CO_3^{2-}]$ ratios [1, 26, 61, 62]. The reduced interaction of the additives with the crystal surface at low $[Ca^{2+}]$:$[CO_3^{2-}]$ ratios also seems to favour the formation of calcite over vaterite [1, 61] at ambient reaction temperatures or vaterite over aragonite at higher reaction temperatures [57].

2.1.1.5 Effect of solvent ratio

The addition of an organic solvent to water affects the electrical conductivity hence ionization of the additive in the solvent mixture [61]. Tang *et al.* [61] showed that with PSSS as additive, the absence of ethanol gave rise to spherical particles with rough surface; 25% ethanol produced spherical vaterite particles with smooth surface and with further increase in ethanol content, flower like and irregular rhombohedral calcite aggregates were produced. Ethanol could therefore strongly affect morphology and polymorph of the $CaCO_3$ products. Formation of aggregates such as vaterite flower shapes (from aggregated plate shapes) and vaterite fluffy aggregates, with increasing alcohol content, has also been reported elsewhere [63].

Highly monodisperse vaterite microspheres with narrow size distributions could be produced via the synergistic effect of an artificial peptide-type block copolymer, poly(ethylene glycol)-*block*-poly(L-glutamic acid) (PEG(110)-b-pGlu(6)), and a mixture of solvents *N,N*-dimethylformamide (DMF) and nonionic water (NIW) at an appropriate ratio [4]. Vaterite spheres with diameter in the range 5.7-6.1 μm were formed at a DMF:NIW v/v ratio of 1:1.4 and vaterite (with trace calcite) spheres with diameter in the range 5.3-6 μm were formed at a ratio of 1:1.

Nonetheless the use of several organic solvents mixed with water in the ratio of solvent to water of 1:4 was found to give different morphologies and polymorphs [64], such as dendrites, flower-like and wheatgrass-like, all of aragonite phase, with glycol, glycerine and glycol methyl ether respectively. Guo *et al.* [6] used DMF/cyclohexanol mixture at different ratios (R) and a polypeptide block copolymer (PEG-b-pAsp) to synthesise multiple layered porous hierarchical structures of vaterite when the R=0.2, layered irregular spherical $CaCO_3$ of vaterite and calcite mixture when R=1, semi spherical particles with centred cavity made of calcite and trace aragonite when R=5 and a twinned bread morphology of ACC was obtained at R=10. Other research has shown that the spontaneous precipitation of $CaCO_3$ using calcium nitrate and sodium bicarbonate solutions, in the presence of 10% v/v ethanol, propanol or diethylene glycol favoured formation of the vaterite phase [65].

2.1.1.6 Effect of mixing mode

Wang *et al.* [1] showed that particle size, shape and distribution depended on the mixing mode of the reaction. Indeed, the particles tend to be smaller and narrowly distributed when the CO_3^{2-} solution was added to the Ca^{2+} solution. However, the opposite procedure created larger particles that were non-uniform in size. This was due to the high initial pH of the carbonate solution at the initial introduction of Ca^{2+}. The high supersaturation generates many nuclei that can grow into relatively larger particles by attracting more free Ca^{2+} ions and consequently, the uniformity of the particles is partially lost.

2.1.1.7 Effect of reaction time

Temporal studies indicate that there are changes in the morphology, polymorph and size of the crystals during the growth process making the reaction time an important parameter to set in the synthesis of $CaCO_3$ particles. By monitoring the reaction of calcium acetate with urea at 90ºC, Chen and Nan [45] recorded that the concentration of flower and hexagonal shaped vaterite decreased while that of rod and cluster shaped aragonite increased up to 100% after

48 hours. An increase in particle size is also normally observed with increasing reaction time [19, 30, 62].

Temporal studies are required to determine the best reaction time to synthesise and stabilise optimum shape and size of particles. It was established [19] that during precipitation reaction with 1 gL^{-1} PSSS additive and pH of 10, loose aggregates of ACC nanoparticles of size 20-40 nm formed after 30 minutes, which further aggregated after 90 minutes. After 120 minutes, spherical particles of size 2-5 μm were formed and at 180 minutes, the number of particles increased sharply to monodispersed particles of average size 8 μm. After 12 h aging, no further change in morphology was observed. Elsewhere, the carbonation precipitation reaction using a small amount (20 ppm) of polyacrylic acid (PAA) polymer produced spherical ACC of size 1 μm after 4 h, which transformed to hollow vaterite spheres of the same size after 10 h [38].

Unstable nanoparticles of ACC form immediately after precipitation. With increase in reaction time (a few hours, as per Table 1), the ACC nanoparticles agglomerate and crystallise into more stable calcite or vaterite phase (or aragonite at high temperatures). Hence to stabilise ACC particles, a short reaction time and an appropriate inhibitor such as Mg are required [66] although high Mg content (24 mol%) has been found to stabilise ACC for up to 14 h [67].

2.1.2 Reverse emulsion

Reverse or water in oil (W/O) or bicontinuous microemulsion is thermodynamic dispersions of water and oil channels stabilised by interfacial layers of surfactants with or without co-surfactants, and consisting of bi-continuous microstructures which can be used as "microreactors" and templates for preparing nanomaterials [68]. The reactants are enclosed inside surfactant micelles that are segregated by the oil phase. When the microemulsions containing CO_3^{2-} and Ca^{2+} ions are mixed, micelles possessing sufficient energy collide and this leads to the mixing of the reactants contained within. This controlled type of precipitation reaction is successful at preparing nano to micro sized particles of varying shapes and morphologies and possessing narrow particle size distributions. Furthermore, the controlled type of precipitation allows for the use of higher reactants concentrations. Reactants concentrations in the range 0.01-0.185 M have been reported [68-71].

The main parameters affecting the morphology, polymorph and size of the particles are the water:surfactant molar ratio (ω), water:oil molar ratio (S), Ca^{2+}:CO_3^{2-} molar ratio (R), pH, reaction temperature and use of additives.

Micelle stability and droplet size in the emulsion depends on the value of ω. The higher the value of ω, the smaller the surfactant concentration and therefore the amount of stable micelles in the emulsion is reduced. Kang *et al.* [72] showed that the maximum ω value depended on the surfactant used. The maximum value of ω for SDS was 600 while much more sodium bis(2-ethylhexyl) sulfosuccinate (AOT) was required for stable micelles formation (maximum ω=30). Tai and Chen [71] reported that, when using sodium triphosphate as additive and AOT as surfactant, the ω value had a greater influence than the S value on the particle size and shape of $CaCO_3$. For example, at all of the S values investigated (1.26, 2.0 and 3.16 respectively), submicron (100-500 nm) sized particles with spherical shape were produced when ω=12.3. Submicron and micron sized discs or irregular shapes were formed when ω=14.0 and 16.0. The size and occurrence of irregular shapes increased further as ω increased due to low surfactant concentration.

The R value had different effects on particle parameters, depending upon the conditions used. Different R values affected the morphology and size of the particles [68, 71] and additional use of additives affected the polymorph of the crystals [70]. Chen and Tai [70] reported doughnut shaped particles of size 1-3 microns at R=1 and 4 and hexagonal plates of diameter 1 micron when R=0.5, all of aragonite phase, when no additives were used and at reaction temperature of 25 ºC (the formation of the aragonite at ambient temperature was attributed to the surfactant (AOT) used, this has also been reported elsewhere [73]). However, with additives, ethylenediamine (EDA) and diethylenetriamine (DETA) at R=1 favoured the formation of calcite crystals. Since the addition of additives increased the pH of the solution, it was concluded that additive or pH and a value of R=1 favoured the formation of calcite.

Similar to solution precipitation systems, high reaction temperature affected the polymorph of the crystals towards the formation of metastable polymorphs aragonite and vaterite [70], however the degree of particle agglomeration increases [70, 74].

A variant of the W/O emulsion method is known as the W/O/W emulsion method, whereby a W/O emulsion containing one reactant is further emulsified in water containing the other reactant. A carrier in the organic phase is responsible for controlled transportation of Ca^{2+} from the external water phase to the internal water phase, to react with CO_3^{2-}. Nano-

sized particles can be synthesised by this method [74, 75] by controlling the water droplet size while the morphology and structure of the particles may be related to the operating concentration levels, the composition of the aqueous phases and the nature of surfactant used for stabilising the emulsions [75].

In summary, biomimetic synthesis is a facile one pot process that enables the synthesis of nano and micro sized dispersed $CaCO_3$ particles with various morphologies and specific polymorphs via the use of different additives and changes in experimental parameters. This allows the particles to have a wide range of applications.

2.2 CO_2 bubbling method

CO_2 bubbling method is the most used industrial process for the production of $CaCO_3$ particles. It involves the use of limestone ($CaCO_3$ rocks), an abundant natural resource to produce slaked lime ($Ca(OH)_2$). Finally CO_2 is bubbled through the $Ca(OH)_2$ to produce $CaCO_3$ particles. CO_2 bubbling is very efficient at producing nano-sized particles [76-85], which are the most sought after size in the industry. However, the polymorphisms that can mainly be achieved are cubic or rhombohedral (atypical of calcite phase) [77-79, 82, 84-87], even in the presence of additives [77-79, 87] or elevated pressures and moderate temperature CO_2 [86, 87]. Also particle agglomeration is rather common [78-81, 84, 86].

Yet, shapes such as spindle [76, 83], needle-like, oval and spheres [81] could be obtained with an appropriate organic additive. Chuajiw *et al.* [81] showed that with diamines of the formula $H_2N(CH_2)_nNH_2$, only vaterite was formed when n=8, aragonite with a small amount of calcite was formed when n=4 and n=6 and vaterite, aragonite and a small amount of calcite was detected when n=2. When amino acids with formula $H_2N(CH_2)_{n-1}COOH$ were used, the main constituent was vaterite while aragonite was detected for precipitated samples with 4-aminobutyric acid ($H_2N(CH_2)_3COOH$) and 6-aminohexanoic acid ($H_2N(CH_2)_5COOH$). Finally with amines, butyamine ($H_2N(CH_2)_3CH_3$) was responsible for the generation of a mixture of aragonite, vaterite and calcite. These results suggest the obvious influence of the type of organic additive and their molecular chain lengths.

The effect of operational parameters was studied using a rotary packed bed (RPB) [84]. The particle size decreased from 66 nm to 45 nm with increase of rotational speed from 500 to 1200 rpm due to large gas-liquid interfacial area which enhanced gas-liquid mass transfer and rapid formation of supersaturated solution of $CaCO_3$ which are favourable for generation of

smaller $CaCO_3$ particles. Increasing the liquid or gas volumetric flow rate also reduced the average particle size because of enhanced gas-liquid mass transfer. Conversely, increasing the initial Ca^{2+} concentration from 0.1 to 0.6 M increased the average particle size from 47 nm to 72 nm, mainly due to an increase in the batch processing time.

Nevertheless, CO_2 bubbling method is simple, cost effective and uses abundant natural resources. The particle size can be easily controlled by adjusting the operational parameters and the particles are nano-sized and can easily be made hydrophilic in situ, by using suitable additives such as [76-78, 80, 83, 88]. Nanometre sizes and dispersibility are very important characteristics required in the paper, paints, coatings and plastics industries.

To summarise the two main synthesis methods, a comparison of the types of particles obtained, experimental procedure and particles' applications for biomimetic and CO_2 bubbling method is presented in Table 5.

Table 5: Comparison between biomimetic and CO_2 bubbling methods

	Biomimetic method	**CO_2 bubbling method**
Polymorph	Either of the polymorphs ACC, calcite, vaterite and aragonite, or a mixture can be stabilised.	Calcite is the main synthesised polymorph.
Morphology	Various morphologies can be synthesised.	Mainly cubic or rhombohedral morphology can be synthesised.
Size	• Nano to micro sized particles. • Monodispersed particles with low particle size distribution can be obtained.	• Mostly nano sized particles. • Particles aggregation is common unless additives are used.
Procedure	• Easy, one pot procedure. • Many experimental parameters (such as pH, temperature, Ca^{2+}:CO_3^{2-} ratio, solvent ratio, additive concentration, additive type, etc.) can be varied to obtain desired polymorph, morphology and size of particles. • Reverse emulsion method can allow controlled reaction and higher reactants concentrations due to separation of reactants.	• Uses readily available limestone to produce $Ca(OH)_2$, making it the current industrial production method. • Synthesis has to be at high pH (due to basic nature of $Ca(OH)_2$). • Synthesis temperature has to be relatively low for high solubility of CO_2 gas.
Applications	Can have wide range of application including as drug delivery vehicles, bone grafting, protein immobilisation, catalysis, biosensors, CO_2 capture and release and water treatment.	Mainly used as a filler for paper, paints, coatings and polymers.

2.3 Other synthesis methods

Other methods for synthesising $CaCO_3$ particles include microwave assisted method, ultrasound assisted method, alternating current method, atomized microemulsion method and spray drying method.

A better alternative to thermal heating could be the use of either microwave or ultrasound assisted technique. Increasing the heating time using microwaves and cellulose as template gave calcite cubes 0.82 μm size after 10 minutes, calcite and vaterite spheres of 1 μm after 20 minutes and calcite and vaterite spheres of 1.24 μm after 30 minutes [89]. On the other hand, different shapes were also observed with varying Ca^{2+} and CO_3^{2-} concentrations using citric acid as additive [90]. At 0.01 M ellipsoidal shape was observed, which changed to peanut-like at >0.02 M and a mixture of both shapes at 0.05 M. The polymorph was all calcite and the size of the particles decreased from 3 to 0.3 μm with increase in concentration from 0.01 to 0.06 M. The effect of solvent mixtures (ethylene glycol (EG) and water) without any additives was also investigated for microwave heating [91]. At low power of 300 W, a ratio of EG:H_2O of 1:9 gave a mixture of calcite and vaterite; a ratio of 1:1 produced almost pure vaterite with ellipse shapes and <4 μm size; a ratio of 9:1 produced porous vaterite spheres with diameter 1-2 μm and having good dispersibility. Increasing the power to 800 W resulted in aragonite nanorods (70-80 nm diameter and 2-3 μm length). Different shapes, phases and particle sizes could also be achieved by varying the intensity and frequency of ultrasound irradiation during $CaCO_3$ synthesis [92, 93]. For instance, aragonite with uniform rod or spindle-like structures was obtained at 50%-70% acoustic amplitude while flower-like vaterite, 3 μm in diameter were synthesised at 75% power [93].

The application of an alternating current through two cells containing Ca^{2+} and CO_3^{2-} and separated by a polytetrafluoroethylene (PTFE) membrane results in different supersaturation around the membrane, enabling crystals to be formed [94]. This method has been used to generate mixtures of micron sized spheroidal vaterite and rhombohedral calcite without the use of additives [94, 95].

Atomisation by spray drying can produce porous spherical and non-spherical particles of <5 μm but a high variation in size is observed [96]. Conversely, the atomized microemulsion polymerisation process could synthesise nanometre sized particles (<100 nm) with $CaCO_3$ core/polymer shell structure [97, 98].

3. Applications of calcium carbonate nano/micro particles

$CaCO_3$ particles has number of applications in various of sectors such as filler materials; for reinforcement and improvement of physical and chemical properties of plastics, paper, paints and coatings, biomedical; for drug/gene delivery, bone regeneration, environmental; for the

design of biosensors and water treatment technology, chemical and food industries. This section will describe selected applications in these areas.

3.1 Filler material

$CaCO_3$ as a filler material can impart extremely useful properties to products such as coatings, paints and pigments, paper, lubricants and plastics.

Calcium carbonate, post-treated with a suitable binder such as stearic acid, can provide superhydrophobic properties when dispersed as filler in coatings (Figure 9 shows the process of producing a superhydrophobic surface). Hydrophobicity of $CaCO_3$ particles has also been achieved in situ during carbonation process using a suitable binder [78, 80]. High contact angles [99, 100] of water droplets (greater than 150°) on the coated surface as well as sliding angles lower than 10° [100, 101] have been reported, which enables the water droplets to easily roll down the surface and at the same time perform self-cleaning action. Moreover, nano- $CaCO_3$ modified by heptadecafluorodecyl trymethoxisilane and an ordinary polyacrylate as the binder was found to have antifreeze properties coupled with its superhydrophobicity [99]. The frost formed on the coated superhydrophobic surface was greatly retarded compared with that on bare copper surface and the surface kept its super hydrophobicity even after freezing-thawing treatment for 10 times.

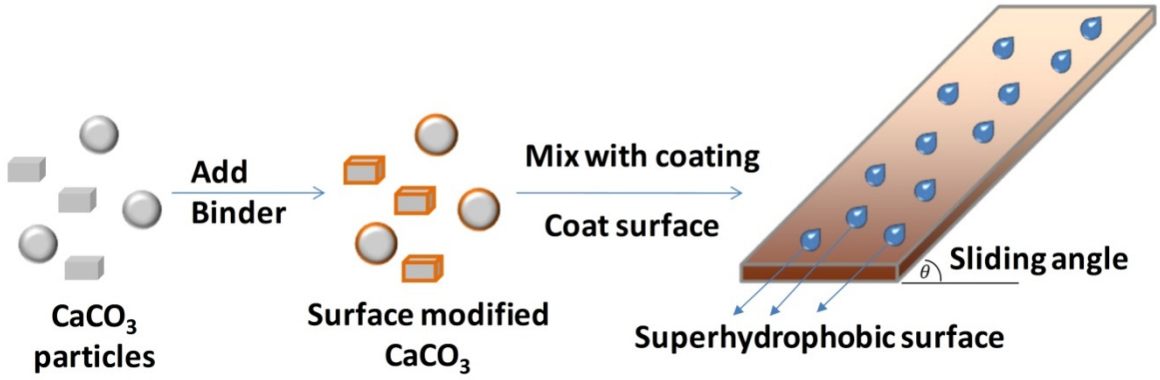

Figure 9: Surface modified $CaCO_3$ particles used as filler in coatings to produce superhydrophobic surfaces

The high dispersibility of nano PCC improved the rheology of liquid coating PVC plastisol (a coating that is used in car underbody paint) [102] and could increase the adhesion and hardness properties of a polyester/epoxy powder coating while also reducing the amount of energy consumption during the curing process of the blend [103].

$CaCO_3$ is used as a filler material in paper so as to improve ink retention, brightness and water resistance. The high porosity and surface area of the $CaCO_3$ particles enhance the

absorption of oils in inks and prevents print rub from occurring [104]. Besides, optimum light scattering for maximum brightness of paper was achieved with a blend of PCC and Al-Mg-silicate compound [105]. Furthermore, water resistance is greatly enhanced with the presence of surface modified $CaCO_3$ [106].

Dispersion of $CaCO_3$ in poly-alpha-olefin (PAO), a lubricant, improved its properties such as friction reduction, high load carrying capacity and anti-wear [107]. This was attributed to a chemical reaction of the $CaCO_3$ nanoparticles during friction to form calcium oxide (CaO) and other organic compounds.

The addition of $CaCO_3$ particles improved the mechanical and rheological properties of a variety of plastics such as poly(L-lactic acid) (PLLA) [108], polyvinylchloride (PVC) [109, 110], polypropylene (PP) [111], PMMA [112], acrylonitrile-butadiene-styrene (ABS) [113], high density polyethylene (HDPE) [114]. Nano-sized particles were generally found to perform better than micro-sized ones due to better dispersion inside the polymer matrix, by increasing the dimensional stability of the material. Also, a wide band gap of 6 ± 0.35 eV and low dielectric constant of 8.19 makes nano sized $CaCO_3$ a suitable filler for outdoor insulators [115].

3.2 Biomedical

The compatibility and non-toxicity of $CaCO_3$ towards the body makes it an attractive drug delivery vehicle resulting in numerous researches being carried out at this effect. Hollow or porous spherical particles are preferred for such applications.

Biomacromolecules and drugs have been successfully loaded inside $CaCO_3$ particles for sustained release in bodily fluids. Fujiwara *et al.* [116] used a W/O/W system with biomacromolecules BSA and DNA dissolved in the aqueous CO_3^{2-} phase to synthesise $CaCO_3$ loaded hollow spheres. A low reaction time of 10 minutes was used so as to encapsulate the biomacromolecules inside vaterite shells. The macromolecules could be released in solution following dissolution or fracture of the microparticles. The drug Betamethasone phosphate (BP) was loaded on $CaCO_3$ during precipitation reaction [117] and resulted in better sustained release in plasma when compared with BP solution. The loading of anticancer drug Doxorubicin Hydrochloride (Dox.HCl) was achieved post precipitation by using $CaCO_3$/carboxymethyl chitosan hybrid micro and nanospheres [118]. The drug loading was realised by the capillary force due to the nanoporous structure of the particles as well as the electrostatic attraction between the negatively charged CMC and positively charged

Dox·HCl. The hybrid particles had high encapsulation capacity and drug release could be effectively sustained. Lysozyme was similarly loaded onto hybrid $CaCO_3$/carboxymethylcellulose microspheres [119]. The porous microspheres had a high adsorption capacity of 450 mg g^{-1}. On the other hand, moderation of the high initial release of the drug Ibuprofen could be achieved by surrounding $CaCO_3$ loaded microparticles with polyelectrolyte multilayer films [18].

Hollow nano-sized spheres synthesised by precipitation with soluble starch was loaded with the anticancer drug Dox and tested for release capacity [27]. Release was undetectable a physiological conditions (pH between 7 and 7.5) for over 48 h and gradually increased around pH 5 and 6, suggesting a good response to the pH values in extracellular sites in tumour tissues and lysosomes in cancer cells, respectively. Hollow spheres have also been reported to be successful at retaining the anti-inflammatory drug naproxen for a period of 27 h, with sustained release [25].

The targeted release of peptides to tumour tissues could be achieved by treating peptide loaded nano $CaCO_3$ with anisamide, a targeting ligand for the sigma receptor which is expressed on lung cells [120]. The nanoparticles could mediate the specific delivery of peptides to tumour tissues *in vivo*, provoking high tumour growth retardation effect with minimal uptake by external organs and no toxic effects. The lipid-$CaCO_3$ calcium core complex was easily dissociated in a low buffer, releasing the peptide in a pH dependent manner. At pH=5.8 (representative of the endosormal environment), the peptide was released in significantly greater amounts while at a pH=7.4 (representative of the bloodstream environment), negligible core dissociation was detected.

$CaCO_3$ particles have also been used as templates for the synthesis of polymeric shells (via layer by layer method) that can encapsulate drugs. The drug containing $CaCO_3$ templates can be easily dissolved at mild conditions such as pH of 2-3 or complexing agents, which do not denature the loaded drug or form toxic complexes with the polymer shells. As a result, the capsules could be designed to: provide sustained release of drugs such as daunorubicin (DNR) and Dox [121], be pH responsive [122, 123], provide multi-compartments for the sequential release of different enzymes at defined positions [124] and electrostatically attract biomacromolecules such as proteins [125]. Figure 10 shows an example of the process of drug loading and unloading on a polymer microcapsule. The $CaCO_3$ loaded with a negatively charged polymer gets dissolved in ethylenediaminetetraacetic acid (EDTA) complexing

agent. The negatively charged polymer remains encapsulated within the mixed polymer shell and electrostatically attracts the positively charged drug during loading. Unloading of the drug proceeds via diffusion mechanism or different environment pH.

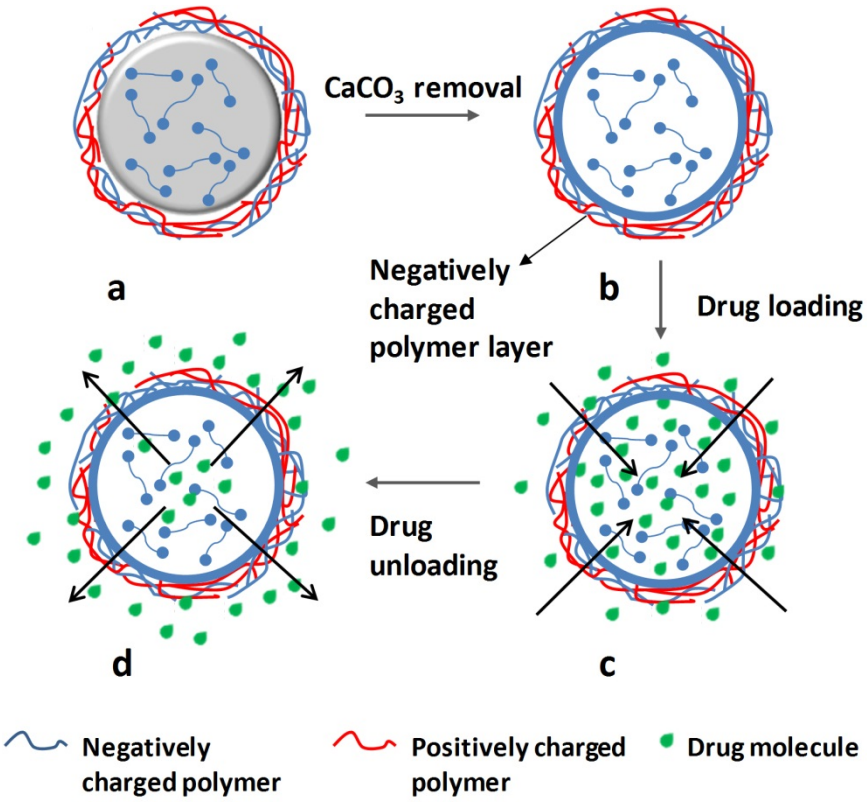

Figure 10: Steps in the synthesis, loading and unloading of drugs into microcapsules: a) Synthesised $CaCO_3$ core loaded with negatively charged polymer and mixed polymer shell microparticle, b) Dissolution of $CaCO_3$, c) Drug loading via electrostatic attraction and d) Drug unloading via diffusion or environment pH.

Alternatively, microcapsules were used to immobilise proteins such as lactabulmin and horseradish peroxidase [126]. These types of micro-reactors can allow small solutes to penetrate the shell wall, while the macromolecules stay in the interior.

Other potential biomedical uses of $CaCO_3$ particles include: aragonite-based material with integrated gentamicin for bone substitution and prevention or treatment of osteomyelitis [127], $CaCO_3$ based toothpastes for right amount of abrasiveness to either enamel or dentine [128] and transdermal delivery of insulin into the blood [129]. The stabilisation of the amorphous phase of $CaCO_3$ is an active research field as it presents an attractive prospect for bone regeneration and healing due to its ability to adapt to any desired shape before it crystallises [130-132]. Furthermore, the relatively high solubility of ACC may be advantageous in the pharmaceutical industry as a drug carrier [133].

Additionally, some synthesised $CaCO_3$ composites had attractive features that allowed easy detection by surface-enhanced Raman scattering (SERS), which is a non-invasive technique for real time monitoring of extracellular matrix development and cell integration in scaffolds for tissue engineering [134], development of degradable guided bone regeneration (GBR) membranes [135] and magnetic properties for targeted delivery of drugs [136].

3.3 Food industry

Various uses have been designed for $CaCO_3$ particles in regards to the food industry, such as biosensors, enzyme supports and catalysis.

$CaCO_3$ nanoparticles have been used as enzyme immobilisation matrix for the construction of xanthine biosensors [137]. Xanthine is a good indicator for estimating fish freshness. The biosensor provided rapid response, high sensitivity, good stability and was successful at avoiding interference of coexisting substances.

$CaCO_3$ proved to be the best support out of all the tested materials for the immobilisation of lipase [138]. The immobilised enzyme was used for the production of monoacylglycerol (MAG), a commonly used surfactant in the food industry, from solid phase glycerolysis of fats and oils. $CaCO_3$ could also be used for the fabrication of calcium alginate beads [139, 140], used for the immobilisation of cells such as bacteria, yeast and fungi in the fermentation process.

Micro-sized $CaCO_3$ showed very good advantages when used as a catalyst for the alcoholysis of fats and oils [141]. The solid catalyst: could be used at high temperatures (>200°C); was not inhibited by the products; resulted in low reaction time and provided essentially complete conversion; did not decrease in activity after weeks of utilisation; had robust structure suitable for use in packed-bed reactors and; could be easily removed from products via screening.

3.4 Environmental

The high porosity and surface area and low mass transport barrier of $CaCO_3$ particles make them an attractive prospect for the design of simple, reliable and cost-effective biosensors and other environmental applications.

The immobilisation of enzymes polyphenol oxidase (PPO) and glucose oxidase have been reported for the detection of phenols [142] and glucose respectively [143]. The PPO/nano- $CaCO_3$

electrode had broad determination range (6×10^{-9} – 2×10^{-5} M), short response time (<12 s), large current density, high sensitivity (474 mA M^{-1}), subnanomolar detection limit (0.44 nM at a signal to noise ratio of 3) and good stability (70% remained after 56 days). The glucose biosensor had similar advantages and was minimally influenced by other compounds at their normal levels, such as ascorbic acid, glutathione, L-cysteine and p-acetaminophenol. However uric acid had a big influence (39%) on the glucose response. The detection mechanism of a biosensor is summarised in Figure 11.

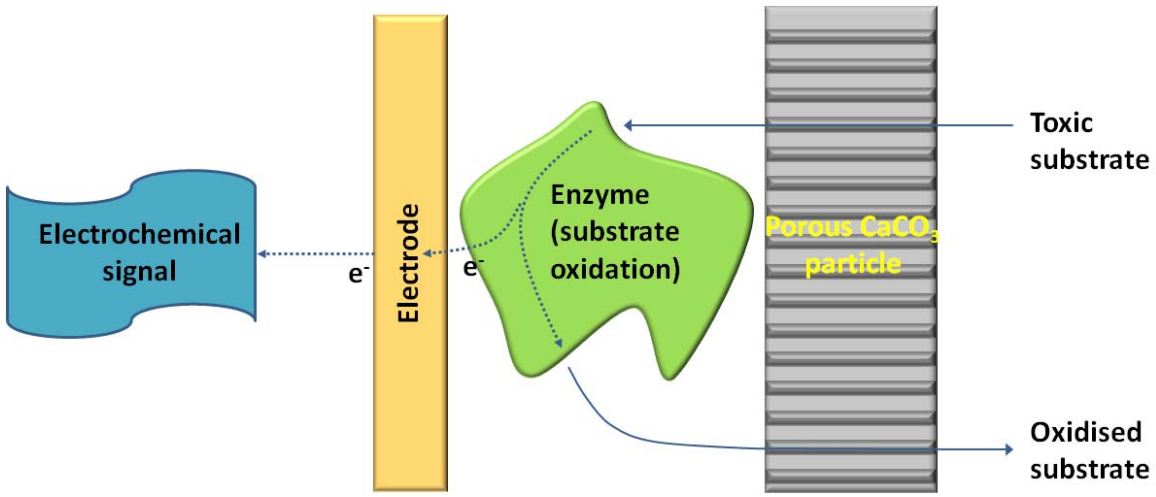

Figure 11: Mechanism of detection of toxic substrate. The substrate molecule penetrates $CaCO_3$ pores and reaches the immobilised enzyme. The enzyme oxidises the substrate by removing electrons, which flow through the electrode and get detected as an electric signal

PAA labelled with aminofluorescin (PAA_{AF}) was co-precipitated with $CaCO_3$, followed by layer by layer encapsulation with polyelectrolyte [144]. The polyelectrolyte capsules (with or without $CaCO_3$ core) could be used as a pH indicator, even when salt was present in solution.

High removal capacities of 515, 1028, 259, 321 and 537 mg g^{-1} of the heavy metals Cd^{2+}, Pb^{2+}, Cr^{3+}, Fe^{3+} and Ni^{2+} respectively, could be achieved from aqueous solutions using precipitated ACC nanoparticles. 83% of trace contaminant, such as radioactive Eu^{3+} could also be achieved. Removal of the metals was via precipitation mechanism, which unfortunately made the ACC non-renewable and necessitated further treatment for the sludge.

$CaCO_3$ can be thermally treated to generate CaO, which can be used for CO_2 capture at moderate carbonation temperature (~650 °C) and release at high calcination temperature (~950 °C) [145-147]. Furthermore, additives such as metakaolin [148], and MgO [149] can be introduced to the CaO so as to improve the regenerability of the CaO by reducing its degree of sintering due to repeated carbonation/calcination cycles.

The photocatalytic splitting of water to liberate oxygen was successfully performed by microwave-based synthesised multi-structured $CaCO_3$/magnetite composite crystals [150]. The magnetic property further allowed for the separation and reuse of the particles.

In summary, $CaCO_3$ can be used as a filler and impart amazing physical properties such as mechanical strength and superhydrophobicity to the material. Being inert, micro or nano sized and porous, it has the ability to be loaded with various compounds and hence act as tremendous vehicles for drugs, proteins and enzymes. Still on the biomedical field, the malleability of ACC makes it an attractive prospect for bone regeneration and healing. $CaCO_3$ can also sustain high temperatures for catalytic reactions. These properties allow a multitude of applications for $CaCO_3$ within a broad range of industries.

4. Conclusions

In this review paper, we have summarised the synthesis approach and potential applications of calcium carbonate particles. The high porosity, surface area to volume ratio, non-toxicity and biocompatibility towards bodily fluids together with the ability of surface modification mean that micro to nano sized $CaCO_3$ particles have a great potential to be used in the field of medicine, catalysis, environment, food processing and material reinforcement as well as improvement of their physical or chemical properties. Current production of nano to micro $CaCO_3$ particles by the CO_2 bubbling method does not have much control over the particle size distribution, shape or phase of the product. However, the biomimetic method offers a facile one pot procedure whereby various sizes (nanometre to micrometre, with narrow particle size distributions), polymorphs and morphologies (spheres, hollow spheres, rods, flowers like, pyramid like) of $CaCO_3$ particles have been successfully synthesised and stabilised *via* the use of additives and adjustments of experimental conditions such as pH and temperature. While the synthesis of basic shapes such as solid and hollow spheres have been established and have been the most tested in applications such as drug storage and delivery, other exotic shapes that have been produced can have potential uses. Some examples are bone grafting, alteration of polymer matrices for the production of "smart" materials, the synthesis of yolk shell particles such as CaO@Carbon or CaO@Silica for applications such as CO_2 capture and catalysis and the assembling of colloids into photonic crystals.

As a result, the synthesis of $CaCO_3$ micro and nano particles is a field that continues to grow in the aim to provide simple and efficient methods for the controlled production of different sizes, polymorphs and morphologies at the industrial scale.

Abbreviations

ABS – Acrylonitrile-butadiene-styrene

AOT – Sodium bis(2-ethylhexyl) sulfosuccinate

BP – Betamethasone phosphate

BSA – Bovine serum albumin

4-BAPTA – 1,2-bis(4-aminophenoxy) ethane-*N*,*N*,*N'*,*N'*-tertraacetic acid

[C_{12}mim]Br – 1-dodecyl-3-methylimidazolium bromide

CTAB – Cetyltrimethylammonium bromide

DDAB – Didodecyldimethylammonium bromide

DDS – Sodium dodecylsulfonate

DETA – Diethylenetriamine

DMC – Dimethyl carbonate

DMF – *N*,*N*-dimethylformamide

DNA – Deoxyribonucleic acid

DNR - Daunorubicin

Dox·HCl – Doxorubicin hydrochloride

DTAB – Dodecyltrimethylammonium bromide

EDA – Ethylenediamine

EDTA – Ethylenediaminetetraacetic acid

EG – Ethylene glycol

HDPE – High density polyethylene

HEC – Hydroxyethyl cellulose

HPCHS – *O*-(hydroxy isopropyl) chitosan

L-Lys – L-lysine

MAG - Monoacylglycerol

MC – Methyl cellulose

$(NH_4)_2CO_3$ – Ammonium carbonate

NIW – Nonionic water

p-aminobenzene sulfonic acid

P123 $[(EO)_{20}$-$(PO)_{72}$-$(EO)_{20}]$– Poly(ethylene oxide)-poly(propylene oxide)-poly(ethylene oxide)

PAA – Polyacrylic acid

PAAL – Poly(acrylic acid)-*block*-(acrylic hydroxyl lactide)

PAM - Polyacrylamide

PAMPSAA – Poly(2-acrylamido-2-methylpropanesulfonic acid-co-acrylic acid)

PAO – Poly-alpha-olefin

PCC – Precipitated calcium carbonate

PEG – Poly(ethylene glycol)

PEG-*b*-pAsp – Poly(ethylene glycol)-*block*-poly(aspartic acid)

PEG(110)-*b*-pGlu(6) – Poly(ethylene glycol)-*block*-poly(L-glutamic acid)

PEG-*b*-PMAA – Poly(ethylene glycol)-*block*-poly(methacrylic acid)

PEO-*b*-PMAA – Poly(ethylene oxide)-*block*-poly(methacrylic acid)

PLLA – Poly(L-lactic acid)

PMMA – Poly(methyl methacrylate)

PP - Polypropylene

PPO – Polyphenol oxidase

PSMA – Poly(styrene-alt-maleic acid)

PS-*b*-PAA – Poly(styrene)-*block*-poly(acrylic acid)

PS-b-PAA-b-PEG – Poly(styrene-*block*-acrylic acid-*block*-ethylene glycol)

PSS – Poly(styrenesulfonate)

PSSS – Poly(sodium-4-styrenesulfonate)

PTFE – Polytetrafluoroethylene

PVC - Polyvinylchloride

PVP - Polyvinylpyrrolidone

SDBS – Sodium dodecylbenzene sulfonate

SDC – Sodium deoxycholate

SDS – Sodium dodecylsulfate

Appendix: Properties of some additives in $CaCO_3$ synthesis

Additive	Molecular Formula	Relative Molecular Mass	Charge
DTAB	$C_{15}H_{34}BrN$	308.3	+
DDAB	$C_{38}H_{80}BrN$	631	+
[C_{12}mim]Br	$C_{14}H_{27}BrN_2$	303.3	+
SDS	$C_{12}H_{25}NaO_4S$	288.4	-
PSSS	[-$CH_2CH(C_6H_4SO_3Na)$-]n	70,000	-
PAA	$(C_3H_4O_2)n$	300,000	Neutral
PVP	$(C_6H_9NO)n$	30,000	Neutral
SDBS	$C_{18}H_{29}NaO_3S$	348.5	-
PSMA	$C_{16}H_{14}Na_2O_8$	120,000	-
CTAB	$C_{19}H_{42}BrN$	364.4	+
PEG	$(C_2H_4O)nH_2O$	10,000	Neutral
L-Lys	$C_6H_{14}N_2O_2$	146.2	Neutral
Phytic acid	$C_6H_{18}O_{24}P_6$	660	-
DMC	$C_3H_6O_3$	90.1	Neutral
SDC	$C_{24}H_{39}NaO_4$	414.6	+

References

1. Y. Wang, Y. X. Moo, C. Chen, P. Gunawan and R. Xu, *J. Colloid Interface Sci.*, 2010, **352**, 393-400.
2. C. Wang, *Mater. Lett.*, 2008, **62**, 2377-2380.
3. Y. W. Wang, Y. Y. Kim, C. J. Stephens, F. C. Meldrum and H. K. Christenson, *Crystal Growth & Design*, 2012, **12**, 1212-1217.
4. X.-H. Guo, S.-H. Yu and G.-B. Cai, *Angew. Chem. Int. Ed.*, 2006, **45**, 3977-3981.
5. Q. Zhang, L. Ren, Y. Sheng, Y. Ji and J. Fu, *Mater. Chem. Phys.*, 2010, **122**, 156-163.
6. X. Guo, L. Liu, W. Wang, J. Zhang, Y. Wang and S.-H. Yu, *CrystEngComm*, 2011, **13**, 2054-2061.
7. A.-W. Xu, M. Antonietti, S.-H. Yu and H. Cölfen, *Adv. Mater.*, 2008, **20**, 1333-1338.
8. Y. Zhao, S. Li, L. Yu, Y. Liu, X. Wang and J. Jiao, *J. Cryst. Growth*, 2011, **324**, 278-283.
9. H. Cölfen and L. Qi, *Chemistry-A European Journal*, 2001, **7**, 106-116.
10. A. Gal, W. Habraken, D. Gur, P. Fratzl, S. Weiner and L. Addadi, *Angew. Chem. Int. Ed.*, 2013, **52**, 4867-4870.
11. I. M. Weiss, N. Tuross, L. Addadi and S. Weiner, *The Journal of experimental zoology*, 2002, **293**, 478-491.
12. L. Addadi, S. Raz and S. Weiner, *Adv. Mater.*, 2003, **15**, 959-970.
13. A. Boettiger, *Real mollusk shells photo*, http://www.berkeley.edu/news/media/releases/2009/04/01_seashells.shtml, Accessed February, 2014.
14. A. Fujii, T. Maruyama, Y. Ohmukai, E. Kamio, T. Sotani and H. Matsuyama, *Colloids and Surfaces A: Physicochemical and Engineering Aspects*, 2010, **356**, 126-133.
15. S. Li, L. Yu, F. Geng, L. Shi, L. Zheng and S. Yuan, *J. Cryst. Growth*, 2010, **312**, 1766-1773.
16. H. Wei, Q. Shen, Y. Zhao, Y. Zhou, D. Wang and D. Xu, *J. Cryst. Growth*, 2005, **279**, 439-446.
17. C. Wang, H. Liu, Q. Gao, X. Liu and Z. Tong, *Carbohydr. Polym.*, 2008, **71**, 476-480.
18. C. Wang, C. He, Z. Tong, X. Liu, B. Ren and F. Zeng, *Int. J. Pharm.*, 2006, **308**, 160-167.

19. M. Lei, W. H. Tang, L. Z. Cao, P. G. Li and J. G. Yu, *J. Cryst. Growth*, 2006, **294**, 358-366.
20. L. Yue, D. Jin, M. Shui and Z. Xu, *Solid State Sciences*, 2004, **6**, 1007-1012.
21. M. Mihai, F. Bucătariu, M. Aflori and S. Schwarz, *J. Cryst. Growth*, 2012, **351**, 23-31.
22. J. Yu, M. Lei, B. Cheng and X. Zhao, *J. Solid State Chem.*, 2004, **177**, 681-689.
23. M. Lei, W. H. Tang and J. G. Yu, *Mater. Res. Bull.*, 2005, **40**, 656-664.
24. H. Cölfen and L. Qi, *Chemistry – A European Journal*, 2001, **7**, 106-116.
25. B. P. Bastakoti, S. Guragain, Y. Yokoyama, S.-i. Yusa and K. Nakashima, *Langmuir*, 2010, **27**, 379-384.
26. X. Yang, G. Xu, Y. Chen, F. Wang, H. Mao, W. Sui, Y. Bai and H. Gong, *J. Cryst. Growth*, 2009, **311**, 4558-4569.
27. W. Wei, G.-H. Ma, G. Hu, D. Yu, T. McLeish, Z.-G. Su and Z.-Y. Shen, *J. Am. Chem. Soc.*, 2008, **130**, 15808-15810.
28. A.-J. Xie, Z.-W. Yuan and Y.-h. Shen, *J. Cryst. Growth*, 2005, **276**, 265-274.
29. B. Cheng, W. Cai and J. Yu, *J. Colloid Interface Sci.*, 2010, **352**, 43-49.
30. Z.-H. Xue, B.-B. Hu, X.-L. Jia, H.-W. Wang and Z.-L. Du, *Mater. Chem. Phys.*, 2009, **114**, 47-52.
31. Q. Shen, H. Wei, Y. Zhao, D.-J. Wang, L.-Q. Zheng and D.-F. Xu, *Colloids and Surfaces A: Physicochemical and Engineering Aspects*, 2004, **251**, 87-91.
32. J. Yu, X. Zhao, B. Cheng and Q. Zhang, *J. Solid State Chem.*, 2005, **178**, 861-867.
33. L. Zhao and J. Wang, *Colloids and Surfaces A: Physicochemical and Engineering Aspects*, 2012, **393**, 139-143.
34. X. Ji, G. Li and X. Huang, *Mater. Lett.*, 2008, **62**, 751-754.
35. L. Qi, J. Li and J. Ma, *Adv. Mater.*, 2002, **14**, 300.
36. G. W. Yan, J. H. Huang, J. F. Zhang and C. J. Qian, *Mater. Res. Bull.*, 2008, **43**, 2069-2077.
37. M. Faatz, F. Gröhn and G. Wegner, *Adv. Mater.*, 2004, **16**, 996-1000.
38. J. Tark Han, X. Xu and K. Cho, *J. Cryst. Growth*, 2007, **308**, 110-116.
39. X.-R. Xu, A.-H. Cai, R. Liu, H.-H. Pan, R.-K. Tang and K. Cho, *J. Cryst. Growth*, 2008, **310**, 3779-3787.
40. L. Zheng, Y. Hu, Y. Ma, Y. Zhou, F. Nie, X. Liu and C. Pei, *J. Cryst. Growth*, 2012, **361**, 217-224.

41. A. W. Xu, Q. Yu, W. F. Dong, M. Antonietti and H. Cölfen, *Adv. Mater.*, 2005, **17**, 2217-2221.
42. K. Gorna, M. Hund, M. Vučak, F. Gröhn and G. Wegner, *Materials Science and Engineering: A*, 2008, **477**, 217-225.
43. D. V. Volodkin, A. I. Petrov, M. Prevot and G. B. Sukhorukov, *Langmuir*, 2004, **20**, 3398-3406.
44. B. Cheng, M. Lei, J. Yu and X. Zhao, *Mater. Lett.*, 2004, **58**, 1565-1570.
45. Z. Chen and Z. Nan, *J. Colloid Interface Sci.*, 2011, **358**, 416-422.
46. H. Tong, W. Ma, L. Wang, P. Wan, J. Hu and L. Cao, *Biomaterials*, 2004, **25**, 3923-3929.
47. Y. Su, H. Yang, W. Shi, H. Guo, Y. Zhao and D. Wang, *Colloids and Surfaces A: Physicochemical and Engineering Aspects*, 2010, **355**, 158-162.
48. S. Kirboga and M. Öner, *Powder Technol.*, 2013, **249**, 95-104.
49. F. Zhang, X. Yang and F. Tian, *Materials Science and Engineering: C*, 2009, **29**, 2530-2538.
50. S. Kim and C. B. Park, *Langmuir*, 2010, **26**, 14730-14736.
51. Y. Pan, X. Zhao, Y. Guo, X. Lv, S. Ren, M. Yuan and Z. Wang, *Mater. Lett.*, 2007, **61**, 2810-2813.
52. M. Yang, X. Jin and Q. Huang, *Colloids and Surfaces A: Physicochemical and Engineering Aspects*, 2011, **374**, 102-107.
53. P. K. Ajikumar, L. G. Wong, G. Subramanyam, R. Lakshminarayanan and S. Valiyaveettil, *Crystal growth & design*, 2005, **5**, 1129-1134.
54. Z. Mao and J. Huang, *J. Solid State Chem.*, 2007, **180**, 453-460.
55. H. Keller and J. Plank, *Cem. Concr. Res.*, 2013, **54**, 1-11.
56. Q. Yu, H.-D. Ou, R.-Q. Song and A.-W. Xu, *J. Cryst. Growth*, 2006, **286**, 178-183.
57. J. Chen and L. Xiang, *Powder Technol.*, 2009, **189**, 64-69.
58. S. Ouhenia, D. Chateigner, M. A. Belkhir, E. Guilmeau and C. Krauss, *J. Cryst. Growth*, 2008, **310**, 2832-2841.
59. A. Chen, P. Ma, Z. Fu, Y. Wu and W. Kong, *J. Cryst. Growth*, 2013, **377**, 136-142.
60. H. Matahwa, V. Ramiah and R. D. Sanderson, *J. Cryst. Growth*, 2008, **310**, 4561-4569.
61. H. Tang, J. Yu, X. Zhao and D. H. L. Ng, *J. Alloys Compd.*, 2008, **463**, 343-349.
62. R. Babou-Kammoe, S. Hamoudi, F. Larachi and K. Belkacemi, *The Canadian Journal of Chemical Engineering*, 2012, **90**, 26-33.

63. G. Yan, L. Wang and J. Huang, *Powder Technol.*, 2009, **192**, 58-64.
64. M. Lei, P. G. Li, Z. B. Sun and W. H. Tang, *Mater. Lett.*, 2006, **60**, 1261-1264.
65. F. Manoli and E. Dalas, *J. Cryst. Growth*, 2000, **218**, 359-364.
66. J. D. Rodriguez-Blanco, S. Shaw, P. Bots, T. Roncal-Herrero and L. G. Benning, *J. Alloys Compd.*, 2012, **536, Supplement 1**, S477-S479.
67. E. Loste, R. M. Wilson, R. Seshadri and F. C. Meldrum, *J. Cryst. Growth*, 2003, **254**, 206-218.
68. Y. Shen, A. Xie, Z. Chen, W. Xu, H. Yao, S. Li, L. Huang, Z. Wu and X. Kong, *Materials Science and Engineering: A*, 2007, **443**, 95-100.
69. F. Rauscher, P. Veit and K. Sundmacher, *Colloids and Surfaces A: Physicochemical and Engineering Aspects*, 2005, **254**, 183-191.
70. C.-K. Chen and C. Y. Tai, *Chem. Eng. Sci.*, 2010, **65**, 4761-4770.
71. C. Y. Tai and C.-k. Chen, *Chem. Eng. Sci.*, 2008, **63**, 3632-3642.
72. S. H. Kang, I. Hirasawa, W.-S. Kim and C. K. Choi, *J. Colloid Interface Sci.*, 2005, **288**, 496-502.
73. S. Thachepan, M. Li, S. A. Davis and S. Mann, *Chem. Mater.*, 2006, **18**, 3557-3561.
74. Q. Sun and Y. Deng, *J. Colloid Interface Sci.*, 2004, **278**, 376-382.
75. T. Hirai, S. Hariguchi, I. Komasawa and R. J. Davey, *Langmuir*, 1997, **13**, 6650-6653.
76. C. Wang, P. Xiao, J. Zhao, X. Zhao, Y. Liu and Z. Wang, *Powder Technol.*, 2006, **170**, 31-35.
77. C. Wang, Y. Liu, H. Bala, Y. Pan, J. Zhao, X. Zhao and Z. Wang, *Colloids and Surfaces A: Physicochemical and Engineering Aspects*, 2007, **297**, 179-182.
78. Y. Chen, X. Ji, G. Zhao and X. Wang, *Powder Technol.*, 2010, **200**, 144-148.
79. L. Xiang, Y. Wen, Q. Wang and Y. Jin, *Mater. Lett.*, 2006, **60**, 1719-1723.
80. L. Du, Y. Wang and G. Luo, *Particuology*, 2013, **11**, 421-427.
81. W. Chuajiw, K. Takatori, T. Igarashi, H. Hara and Y. Fukushima, *J. Cryst. Growth*, 2014, **386**, 119-127.
82. G. Wu, Y. Wang, S. Zhu and J. Wang, *Powder Technol.*, 2007, **172**, 82-88.
83. C. Wang, Y. Sheng, X. Zhao, Y. Pan, B. Hari and Z. Wang, *Mater. Lett.*, 2006, **60**, 854-857.
84. B.-C. Sun, X.-M. Wang, J.-M. Chen, G.-W. Chu, J.-F. Chen and L. Shao, *Chem. Eng. J.*, 2011, **168**, 731-736.

85. C. Wang, J. Zhao, X. Zhao, H. Bala and Z. Wang, *Powder Technol.*, 2006, **163**, 134-138.
86. C. Domingo, J. García-Carmona, E. Loste, A. Fanovich, J. Fraile and J. Gómez-Morales, *J. Cryst. Growth*, 2004, **271**, 268-273.
87. C. Zhang, J. Zhang, X. Feng, W. Li, Y. Zhao and B. Han, *Colloids and Surfaces A: Physicochemical and Engineering Aspects*, 2008, **324**, 167-170.
88. L. Hu, P. Dong and G. Zhen, *Mater. Lett.*, 2009, **63**, 373-375.
89. L. H. Fu, Y. Y. Dong, M. G. Ma, S. M. Li and R. C. Sun, *Ultrason. Sonochem.*, 2013, **20**, 839-845.
90. R. Rodríguez-Clemente and J. Gómez-Morales, *J. Cryst. Growth*, 1996, **169**, 339-346.
91. Y. Chen, X. Ji and X. Wang, *J. Cryst. Growth*, 2010, **312**, 3191-3197.
92. Y. Kojima, K. Yamaguchi and N. Nishimiya, *Ultrason. Sonochem.*, 2010, **17**, 617-620.
93. G.-T. Zhou, C. Y. Jimmy, X.-C. Wang and L.-Z. Zhang, *New J. Chem.*, 2004, **28**, 1027-1031.
94. J. Watanabe and M. Akashi, *Acta Biomaterialia*, 2009, **5**, 1306-1310.
95. J. Watanabe and M. Akashi, *J. Colloid Interface Sci.*, 2008, **327**, 44-50.
96. K. Cho, Y. J. Suh, H. Chang, D. S. Kil, B. G. Kim and H.-D. Jang, *Adv. Powder Technol.*, 2010, **21**, 145-149.
97. S. Mishra, A. Chatterjee and R. Singh, *Polym. Adv. Technol.*, 2011, **22**, 2571-2582.
98. A. Chatterjee and S. Mishra, *Particuology*, 2013, **11**, 760-767.
99. H. Wang, L. Tang, X. Wu, W. Dai and Y. Qiu, *Appl. Surf. Sci.*, 2007, **253**, 8818-8824.
100. H. Zhang, X. Zeng, Y. Gao, F. Shi, P. Zhang and J.-F. Chen, *Industrial & Engineering Chemistry Research*, 2011, **50**, 3089-3094.
101. Z. Hu and Y. Deng, *Industrial & Engineering Chemistry Research*, 2010, **49**, 5625-5630.
102. H. Zhang, J. Chen, H. Zhou, G. Wang and J. Yun, *J. Mater. Sci. Lett.*, 2002, **21**, 1305-1306.
103. M. Kalaee, S. Akhlaghi, A. Nouri, S. Mazinani, M. Mortezaei, M. Afshari, D. Mostafanezhad, A. Allahbakhsh, H. A. Dehaghi and A. Amirsadri, *Prog. Org. Coat.*, 2011, **71**, 173-180.
104. H. Koivula, M. Toivakka and P. Gane, *J. Colloid Interface Sci.*, 2012, **369**, 426-434.
105. M. Juuti, K. Koivunen, M. Silvennoinen, H. Paulapuro and K.-E. Peiponen, *Colloids and Surfaces A: Physicochemical and Engineering Aspects*, 2009, **352**, 94-98.

106. Z. Hu, X. Zen, J. Gong and Y. Deng, *Colloids and Surfaces A: Physicochemical and Engineering Aspects*, 2009, **351**, 65-70.
107. M. Zhang, X. Wang, X. Fu and Y. Xia, *Tribology international*, 2009, **42**, 1029-1039.
108. J.-Z. Liang, L. Zhou, C.-Y. Tang and C.-P. Tsui, *Composites Part B: Engineering*, 2013, **45**, 1646-1650.
109. C. H. Chen, C. C. Teng, S. F. Su, W. C. Wu and C. H. Yang, *J. Polym. Sci., Part B: Polym. Phys.*, 2006, **44**, 451-460.
110. I. Kemal, A. Whittle, R. Burford, T. Vodenitcharova and M. Hoffman, *Polymer*, 2009, **50**, 4066-4079.
111. A. Afshar, I. Massoumi, R. L. Khosh and R. Bagheri, *Materials & Design*, 2010, **31**, 802-807.
112. M. Avella, M. E. Errico and E. Martuscelli, *Nano Lett.*, 2001, **1**, 213-217.
113. L. Jiang, Y. Lam, K. Tam, T. Chua, G. Sim and L. Ang, *Polymer*, 2005, **46**, 243-252.
114. S. Sahebian, S. Zebarjad, J. V. Khaki and S. Sajjadi, *J. Mater. Process. Technol.*, 2009, **209**, 1310-1317.
115. G. Momen and M. Farzaneh, *Rev. Adv. Mater. Sci*, 2011, **27**, 1-13.
116. M. Fujiwara, K. Shiokawa, K. Morigaki, Y. Zhu and Y. Nakahara, *Chem. Eng. J.*, 2008, **137**, 14-22.
117. Y. Ueno, H. Futagawa, Y. Takagi, A. Ueno and Y. Mizushima, *J. Controlled Release*, 2005, **103**, 93-98.
118. J. Wang, J.-S. Chen, J.-Y. Zong, D. Zhao, F. Li, R.-X. Zhuo and S.-X. Cheng, *The Journal of Physical Chemistry C*, 2010, **114**, 18940-18945.
119. Z. Lu, J. Zhang, Y. Ma, S. Song and W. Gu, *Materials Science and Engineering: C*, 2012, **32**, 1982-1987.
120. S. K. Kim, M. B. Foote and L. Huang, *Cancer Letters*, 2012.
121. Q. Zhao, S. Zhang, W. Tong, C. Gao and J. Shen, *Eur. Polym. J.*, 2006, **42**, 3341-3351.
122. A. A. Antipov, D. Shchukin, Y. Fedutik, A. I. Petrov, G. B. Sukhorukov and H. Möhwald, *Colloids and Surfaces A: Physicochemical and Engineering Aspects*, 2003, **224**, 175-183.
123. Q. Zhao and B. Li, *Nanomedicine: Nanotechnology, Biology and Medicine*, 2008, **4**, 302-310.
124. H. Bäumler and R. Georgieva, *Biomacromolecules*, 2010, **11**, 1480-1487.

125. G. B. Sukhorukov, D. V. Volodkin, A. M. Gunther, A. I. Petrov, D. B. Shenoy and H. Mohwald, *J. Mater. Chem.*, 2004, **14**, 2073-2081.
126. D. V. Volodkin, N. I. Larionova and G. B. Sukhorukov, *Biomacromolecules*, 2004, **5**, 1962-1972.
127. A. Lucas-Girot, M. C. Verdier, O. Tribut, J. C. Sangleboeuf, H. Allain and H. Oudadesse, *Journal of Biomedical Materials Research Part B: Applied Biomaterials*, 2005, **73**, 164-170.
128. M. Pickles, M. Evans, C. Philpotts, A. Joiner, R. Lynch, N. Noel and M. Laucello, *International dental journal*, 2005, **55**, 197-202.
129. M. Higaki, M. Kameyama, M. Udagawa, Y. Ueno, Y. Yamaguchi, R. Igarashi, T. Ishihara and Y. Mizushima, *Diabetes technology & therapeutics*, 2006, **8**, 369-374.
130. N. A. J. M. Sommerdijk, E. N. M. v. Leeuwen, M. R. J. Vos and J. A. Jansen, *CrystEngComm*, 2007, **9**, 1209-1214.
131. J. J. Donners, B. R. Heywood, E. W. Meijer, R. J. Nolte and N. A. Sommerdijk, *Chemistry (Weinheim an der Bergstrasse, Germany)*, 2002, **8**, 2561-2567.
132. D. C. Popescu, E. N. van Leeuwen, N. A. Rossi, S. J. Holder, J. A. Jansen and N. A. Sommerdijk, *Angewandte Chemie (International ed. in English)*, 2006, **45**, 1762-1767.
133. S. Raz, P. C. Hamilton, F. H. Wilt, S. Weiner and L. Addadi, *Adv. Funct. Mater.*, 2003, **13**, 480-486.
134. I. Y. Stetciura, A. V. Markin, A. N. Ponomarev, A. V. Yakimansky, T. S. Demina, C. Grandfils, D. V. Volodkin and D. A. Gorin, *Langmuir*, 2013, **29**, 4140-4147.
135. K. Fujihara, M. Kotaki and S. Ramakrishna, *Biomaterials*, 2005, **26**, 4139-4147.
136. M. Mihai, V. Socoliuc, F. Doroftei, E.-L. Ursu, M. Aflori, L. Vekas and B. C. Simionescu, *Crystal Growth & Design*, 2013, **13**, 3535-3545.
137. D. Shan, Y. Wang, H. Xue and S. Cosnier, *Sensors and Actuators B: Chemical*, 2009, **136**, 510-515.
138. R. Rosu, Y. Uozaki, Y. Iwasaki and T. Yamane, *Journal of the American Oil Chemists' Society*, 1997, **74**, 445-450.
139. A. Groboillot, D. Boadi, D. Poncelet and R. Neufeld, *Crit. Rev. Biotechnol.*, 1994, **14**, 75-107.
140. L. Chan, H. Lee and P. Heng, *Int. J. Pharm.*, 2002, **242**, 259-262.
141. G. Suppes, K. Bockwinkel, S. Lucas, J. Botts, M. Mason and J. Heppert, *Journal of the American Oil Chemists' Society*, 2001, **78**, 139-146.

142. D. Shan, M. Zhu, E. Han, H. Xue and S. Cosnier, *Biosens. Bioelectron.*, 2007, **23**, 648-654.
143. D. Shan, M. Zhu, H. Xue and S. Cosnier, *Biosens. Bioelectron.*, 2007, **22**, 1612-1617.
144. D. Haložan, U. Riebentanz, M. Brumen and E. Donath, *Colloids and Surfaces A: Physicochemical and Engineering Aspects*, 2009, **342**, 115-121.
145. N. H. Florin and A. T. Harris, *Industrial & Engineering Chemistry Research*, 2008, **47**, 2191-2202.
146. G. S. Grasa, J. C. Abanades, M. Alonso and B. González, *Chem. Eng. J.*, 2008, **137**, 561-567.
147. Z. Yang, M. Zhao, N. H. Florin and A. T. Harris, *Industrial & Engineering Chemistry Research*, 2009, **48**, 10765-10770.
148. K. Wang, X. Guo, P. Zhao and C. Zheng, *Applied Clay Science*, 2010, **50**, 41-46.
149. W. Liu, B. Feng, Y. Wu, G. Wang, J. Barry and J. o. C. Diniz da Costa, *Environmental science & technology*, 2010, **44**, 3093-3097.
150. D. Walsh, Y.-Y. Kim, A. Miyamoto and F. C. Meldrum, *Small*, 2011, **7**, 2168-2172.

Table of Contents

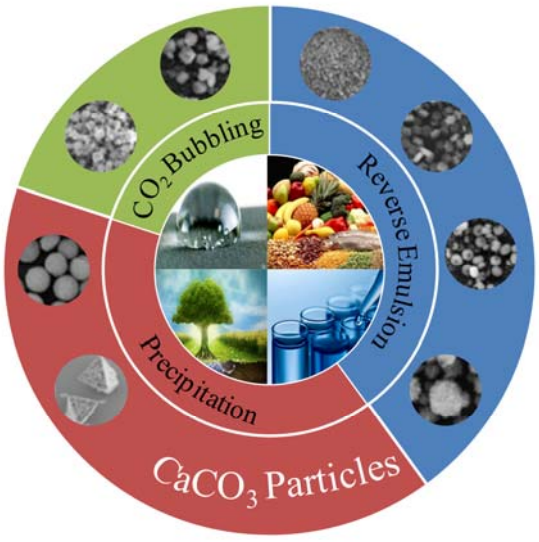

This paper is an authoritative review of the synthesis of nano and micro sized calcium carbonate particles and their applications.